PL-TR-95-2065

ULTRAVIOLET ARRAY DETECTOR RESEARCH

Michael Gangl
Michael Bullinger
Richard Cundiff
Jack McKay
John Middlestadt
Wendy Nicholas

Research Support Instruments, Inc
318 Clubhouse Lane
Hunt Valley, Maryland 21031-1323

30 April 1995

Final Report
31 January 1992-12 June 1995

PHILLIPS LABORATORY
Directorate of Geophysics
AIR FORCE MATERIEL COMMAND
HANSCOM AFB, MA 01731-3010

"This technical report has been reviewed and is approved for publication"

JOSEPH LARRABEE
Contract Manager

DAVID N. ANDERSON
Branch Chief

WILLIAM K. VICKERY
Division Director

This report has been reviewed by the ESC Public Affairs Office (PA) and is releasable to the National Technical Information Service (NTIS).

Qualified requestors may obtain additional copies from the Defense Technical Information Center (DTIC). All others should apply to the National Technical Information Service (NTIS).

If your address has changed, if you wish to be removed from the mailing list, or if the addressee is no longer employed by your organization, please notify PL/TSI, 29 Randolph Road, Hanscom AFB, MA 01731-3010. This will assist us in maintaining a current mailing list.

Do not return copies of this report unless contractual obligations or notices on a specific document requires that it be returned.

REPORT DOCUMENTATION PAGE

Form Approved
OMB No. 0704-0188

1. AGENCY USE ONLY *(Leave blank)*	2. REPORT DATE	3. REPORT TYPE AND DATES COVERED
	30 April 1995	FINAL (31 Jan 1992-12 Jun 1995)

4. TITLE AND SUBTITLE
Ultraviolet Array Detector Research

5. FUNDING NUMBERS
PE 62101F
PR A321 TA06 WU AG
Contract F19628-89-C-0147

6. AUTHOR(S)
Michael Gangl, Michael Bullinger, Rich Cundiff, Jack McKay, John Middlestadt, Wendy Nicholas

7. PERFORMING ORGANIZATION NAME(S) AND ADDRESS(ES)
RESEARCH SUPPORT INSTRUMENTS, INC.
318 Clubhouse Lane
Hunt Valley, Maryland 21031-1323

8. PERFORMING ORGANIZATION REPORT NUMBER

9. SPONSORING/MONITORING AGENCY NAME(S) AND ADDRESS(ES)
PHILLIPS LABORATORY
29 Randolph Road
Hanscom AFB, MA 01731-3010
Contract Manager: J.C.Larrabee/GPIM

10. SPONSORING/MONITORING AGENCY REPORT NUMBER
PL-TR-95-2065

11. SUPPLEMENTARY NOTES

12a. DISTRIBUTION/AVAILABILITY STATEMENT
Approved for public release; distribution unlimited.

12b. DISTRIBUTION CODE

13. ABSTRACT *(Maximum 200 words)*

Under this contract multiple tasks were performed in support of the development of Ultraviolet Array Detector Research. The Horizon Ultraviolet Program instrumentation was supported through a second Space shuttle launch. An Ebert-Fastie spectrometer was modified to incorporate an array detector, as well as an astigmatic grating study performed for this instrument to determine performance improvement with the array over previously used detection techniques. The Auroral Ultraviolet Radiance Analyzer satellite payload was developed and prepared for satellite launch. The design and technical approach for these instruments, along with measured results, were presented in a scientific paper.

14. SUBJECT TERMS	15. NUMBER OF PAGES
Ultraviolet sensing, Atmospheric Remote Sensing, Array Detector	68
	16. PRICE CODE

17. SECURITY CLASSIFICATION OF REPORT	18. SECURITY CLASSIFICATION OF THIS PAGE	19. SECURITY CLASSIFICATION OF ABSTRACT	20. LIMITATION OF ABSTRACT
Unclassified	Unclassified	Unclassified	SAR

Table of Contents

1.0 Introduction 1

2.0 Description of Tasks 1
- 2.1 HUP Refurbishment 1
- 2.2 Ground-based Photometer Assemblies 1
- 2.3 Linear Array with Ebert-Fastie Spectrometer 2
- 2.4 Support of AURA for STEP Mission 2 Meetings 2
- 2.5 Investigation of Astigmatic Grating for Ebert-Fastie Spectrometers 2
- 2.6 SPIE Paper on AURA Experiment 3
- 2.7 AURA Slit Design 3
- 2.8 AURA Scan Mirror Assembly Analysis 3
- 2.9 Fiducial Tests 3
- 2.10 Microcontroller Development 4
- 2.11 PMT Purchases 4
- 2.12 Thermal Analysis of Integrated Detector PC Board 5

3.0 Contributing Personnel 5

Appendix A Linear Array Detector Development 7

Appendix B AURA, An Experiment to Measure Ultraviolet Radiation of the Earth's Atmosphere from Space, SPIE San Diego Conference, 1992 15

Appendix C Evaluation of Honeywell Reflective Optoelectronic Sensor, HOA1160-001 27

Appendix D System Controller Development Work 51

Appendix E Thermal Analysis of the Pulse Amplifier/Discriminator Board in the Integrated Detector Assembly 59

1.0 Introduction

This is the final report for the BAA program F19628-89-C-0147 and satisfies CDRL items 104 & 105. This report will describe the technical achievements of RSI on the contract. The program was a means of providing PL/GPIM with engineering, manufacturing, and test support. Since the tasks performed are varied, they will each be addressed separately. The majority of the tasks were in support of the AURA program, currently under development.

2.0 Description of Tasks

2.1 HUP Refurbishment

The Horizon Ultraviolet Program (HUP) instrument required modification. This modification was allowed by the Space Systems Division due to the launch delay of the 675 assembly. There were two main issues which were addressed. The first is that the spectrometer entrance slit size was incorrect. The resolution was 20 Å and the slit should have been for a 5 Å bandwidth. Also, the latch assembly indication signal failed to return a proper signal when the latch assembly had properly engaged.

The assembly was returned to RSI where the proper entrance slit was placed into the spectrometer. An investigation into the latch signal problem revealed that the fiducial indicator was triggered when the latch mechanism was engaged. However, the drive would backlash enough in the locked position for the fiducial to see light and indicate an unlatched position. This occurred only under certain gravitational orientations of the mechanism. The problem could have been fixed in software, but since the problem appeared to be only an annoyance during ground testing it was decided not to risk modifying the software and changing the EPROM's.

After changing the entrance slit, the assembly was taken to Fairchild Space where it was vibrated (random test) and thermal tested. The vibration required a modified test fixture at Fairchild. The unit was then returned for integration into the launch vehicle.

2.2 Ground-based Photometer Assemblies

Two ground-based photometers, RSI model 010-224-01 were built on the contract. These photometers consist of a cylindrical housing containing an EMR 541N photomultiplier tube and an RSI 470-209 high voltage and pulse amplifier/discriminator assembly. Also included was a set of 50 foot cables, 710-224-10 and 710-224-11, and a documentation package of the assembly drawings, test reports, and wiring schematics.

2.3 Linear Array with Ebert-Fastie Spectrometer

As part of a joint effort to advance the instrument capabilities of the spectrometers, PL/GPIM authorized RSI to mount a EG&G Reticon linear silicon diode array to an Ebert-Fastie spectrometer. The idea was to expand the existing spectrometer technology to include simultaneous spectral coverage over the desired wavelength band. This would either eliminate the requirement for a mechanism to rotate the grating, or in conjunction with the grating mechanism provide multiple spectral windows.

RSI integrated the Reticon detector array to the spectrometer via a modified exit plane and designed and built an electronics board to collect the information and transfer it to a computer. A user functional software program presented the collected spectral information on the computer. The details of the work performed for this task are outlined in Appendix A.

A task option that was not exercised was to integrate an area array detector to the Ebert-Fastie spectrometer. This upgraded system would include an astigmatic grating (see below) with one of the spectrometers that PL/GPIM has in storage. The detector would be a CCD area array with an Image Intensifier for operation in the ultaviolet spectrum. This system would be an economical upgrade for an instrument which already has a long history of successful operation in space.

2.4 Support of AURA for STEP Mission 2 Meetings

A set of meetings was held at TRW facilities in Virginia for the Space Test Experiment's Platform (STEP) planned mission 2 (actually the third planned mission). The Atmospheric Ultraviolet Radiance Analyzer (AURA) experiment was a candidate for this satellite at the time. The actual contract for AURA had not been awarded at the time of the meetings. RSI, as the experiment's hardware designer and manufacturer, were required to provide support for PL/GPIM at the meetings. RSI met with TRW and DSI personnel as well as communicating with them via telephone conversations after the meetings.

The AURA experiment was removed as a candidate for Mission 2. Subsequent meetings were held under the AURA contract for Mission 3. While the meetings and correspondence did not result in a flight for AURA, RSI learned valuable information on STEP requirements that will assist us in providing TRW with accurate information at less cost when a Mission for AURA is identified.

2.5 Investigation of Astigmatic Grating for Ebert-Fastie Spectrometers

RSI reviewed the possibility of replacing the Ebert-Fastie spectrometer grating with an astigmatic version. This plane grating is slightly curved to provide a corrected point image at the focal plane, thus allowing for uniform spectral resolution with a linear array such as that described above. While PL/GPIM did not opt to have us build and assemble a spectrometer with the astigmatic grating, the information is now available for future instrument considerations.

2.6 SPIE Paper on AURA Experiment

RSI co-authored a paper with Dr. Richard Eastes for SPIE, the optical engineering society and presented the paper at the SPIE conference in San Diego in 1992. The paper described the mission goals of the experiment and the design of the hardware (at that time) to meet those goals. A copy of the paper is attached as Appendix B.

2.7 AURA Slit Design

As part of the effort to utilize this BAA program to support the AURA contract, a new exit slit assembly was designed for the AURA spectrometers. This redesign was requested so as to provide the maximum slit height possible for the existing assembly. The result was to increase the slit height to 8 millimeters and extend the photomultiplier tube (PMT) out of the integrated detector housing to bring the photocathode active area as close as possible to the slit focal plane. The assembly is now limited by the photocathode active area, the distance from the entrance window of the PMT to that area, and the F# of the spectrometer. Therefore, since these factors are not subject to change, the slit height has been maximized for this system.

2.8 AURA Scan Mirror Assembly Analysis

The scan mirror assembly includes some key functions that required additional analysis to determine their feasibility in the design. The gear tooth profile was analyzed to determine the effects of variances of the mesh on pointing accuracy. It has been determined that the variances with the gears chosen did not significantly contribute to pointing inaccuracy.

The "footprint" of the instrument in the atmosphere resulting from the imaging of the spectrometer slit was analyzed. Imaging at altitudes from earth where expected UV emissions are anticipated were calculated and the results were presented to Dr. Eastes.

One of the more complex aspects of the scan mirror housing design has been the field-of-view of the sun sensors and their imaging with respect to the instrument field-of-view. Beam 4 analysis provided an insight to the effect of baffling and side reflection viewing off the scan mirror. The result is that the sun sensors do not see a simple footprint area encompassing the instrument view. Rather, the two sun sensors will provide early warning of impending sun light in the scan directions (one left, one right) but are severely restricted in the spacecraft velocity direction. Since it is somewhat improbable that the spacecraft will fly into a viewing angle of the sun (on the nadir side of the satellite), it is not a significant risk to use the sun sensors in this manner. The sun sensors are a second layer of sun protection, the first being the viewing functions programmed from the ground station. This analysis has been presented to Dr. Eastes.

2.9 Fiducial Tests

In the past, the fiducial assemblies were limited to the transmissive types that relied on a hole in a rotating disk that provided a light path from an LED to a phototransistor.

While this method has been used extensively it poses some challenging design issues. These include alignment of the transmitter to the receiver and the spacing of the fiducial assemblies to the rotating disk.

RSI proposed to use reflective fiducials in the scan mirror assemblies on the AURA program as an alternative. The light from the LED is focused to a plane located in front of the assembly, which is also the focal plane for the phototransistor. The switching is obtained from reflecting or not reflecting the light back up into the assembly from a reflective surface on a disk. These fiducials are purchased in their own housing, pre-aligned. This eliminates the necessity of aligning them at the assembly level. However, there are several questions that remain. First, what is the tolerance on the distance from the fiducial assembly to the reflective disk? Second, what is the spot size at the disk plane for switching resolution? And third, how reflective does the surface need to be to adequately reflect the light?

In Appendix C, the Honeywell reflective fiducials were evaluated against these criterion. The results are that the reflective fiducials are less difficult to align relative to the disk, provide adequate switching resolution, and are much more tolerant to various reflective surface qualities that expected. This last point is important due to predicted surface degradation from radiation in space. The fiducial housing is manufactured from a NASA suggested, low outgassing Acetal Copolymer material. The reflective fiducials are now planned to be used in the AURA program.

2.10 Microcontroller Development

The AURA experiment is using a sophisticated processing system to collect data from the instruments and relay the information to the spacecraft. The heart of the processor is the Motorola 68332 microcontroller. This device contains many of the functions required of the experiment without all the peripheral components needed for a less sophisticated microprocessor. These include the bidirectional asynchronous command link, the synchronous telemetry link, and the stepper motor phase controls,among others.

RSI built and tested a breadboard version of the System Controller that will fly in the AURA experiment. This allowed for testing of the design prior to PC board manufacturing. It also permitted the testing of the 68332 microcontroller and other key design elements, including the field-programmable gate array (FPGA). The results of this testing are explained in Appendix D.

2.11 PMT Purchases

Two new photomultiplier tubes (PMT) were purchased for the AURA contract. These EMR 541G PMT's, serial numbers 79879 and 80243, have better than expected quantum efficiencies and have been calibrated at the PL/GPIM facility. They will be used in the integrated detector packages to fly on the AURA experiment.

2.12 Thermal Analysis of Integrated Detector PC Board

Due to PL/GPIM's previous experience with a possible failed integrated detector package in a flight mission, it was requested that RSI provide a thermal analysis to determine if there is a inherent thermal dissipation problem with the assembly that can be rectified prior to the launch of the AURA experiment. The PC board was modeled and the resulting analysis is described in Appendix E. The initial results were discouraging. But as the addendum explains, when the trace metallization on the PC board is accounted for the board does not have a heat dissipation problem. Therefore, there will not be a "localized" heating of a component decreasing its long term stability.

3.0 Contributing Personnel

Michael Gangl
Michael Bullinger
Richard Cundiff
Jack McKay
John Middlestadt
Wendy Nicholas

(blank)

Appendix A

Linear Array Detector Development

1.0 Introduction

RSI adapted an Ebert/Fastie spectrometer with a linear array detector in an effort to eliminate the scanning mechanism for the spectrometer's grating. The linear array detector provides multispectral information without moving the grating. Photomultiplier tube (PMT) detectors, used in previous RSI spectrometers, provide data for only one wavelength at each grating position.

The linear array detector system and test setup are shown in Figure 1. A Mercury source is directed through a telescope to the Ebert/Fastie Spectrograph. The diffracted light charges the photodiodes of the Reticon linear array detector. A more detailed diagram of the spectrograph linear array and support electronics is shown in Figure 2. The EG&G Reticon linear array was selected for this research because of the reputation of the company as well as its willingness to provide technical information. Data from the linear array is transferred via a video output to an interface card designed by RSI. This interface card digitizes the spectral data so that the PC may read and display it.

Figure 3 presents the data as it appears on the PC's monitor. The dotted line from the interface card to the spectrometer represents hardware that is still under development. This hardware will allow the PC to read fiducial inputs and control stepper motors.

Design of this system involved three major tasks: mechanical support of the Reticon linear array and electronics, hardware design of the PC/Reticon array interface card, and software development for the interface.

2.0 Spectrograph/Reticon Interface Mounting Plate

Mounting the Reticon linear array and support electronics required modification of the spectrograph front plate and housing. Also, a custom machined enclosure was developed to house the electronics (see Figure 2).

The standard RSI Ebert/Fastie Spectrometer front plate supports the photomultiplier tube detector. The entrance slit is the same size as the exit silt. The original front plate was modified to accommodate the Reticon linear array. A hole was cut for the linear array and mounting holes were adjusted. Because of the increase in slit size, a slot had to be cut in the spectrometer housing. Figure 4 shows the details of this housing modification.

3.0 Interface Hardware

The Reticon linear array was mounted on a vectorboard at the spectrometer from plate, and 26 gauge wire was run to the support electronics (see Figure 2). A video output and timing signals from the Reticon support electronics connect to the RSI interface board. Refer to the block diagram in Figure 5.

After a Reticon Sync pulse, an A/D conversion is started at every other master clock (master clock + 2). Each A/D conversion is read by the PC. The PC receives data for the 512 array pixels before the next Sync pulse. The data is presented in graphical from on the PC's monitor (see Figure 3).

The input buffer interfaces the linear array's timing signals as well as fiducial states (on/off) to the PC bus. Output buffers allow PC drive and control of the spectrometer's grating and dust cover stepper motors. In Figure 5, the dotted lines enclose the PC interface electronics that have been built by RSI, but have not been fully integrated with the spectrometer.

4.0 Software

Figure 8 is a software flow chart for the Reticon linear array/PC interface. The software, at this time, does not read the fiducial inputs or drive the stepper motor outputs shown in the block diagram of Figure 5. It is written in Turbo Pascal 5.5 using the Borland Graphics Interface (BGI).

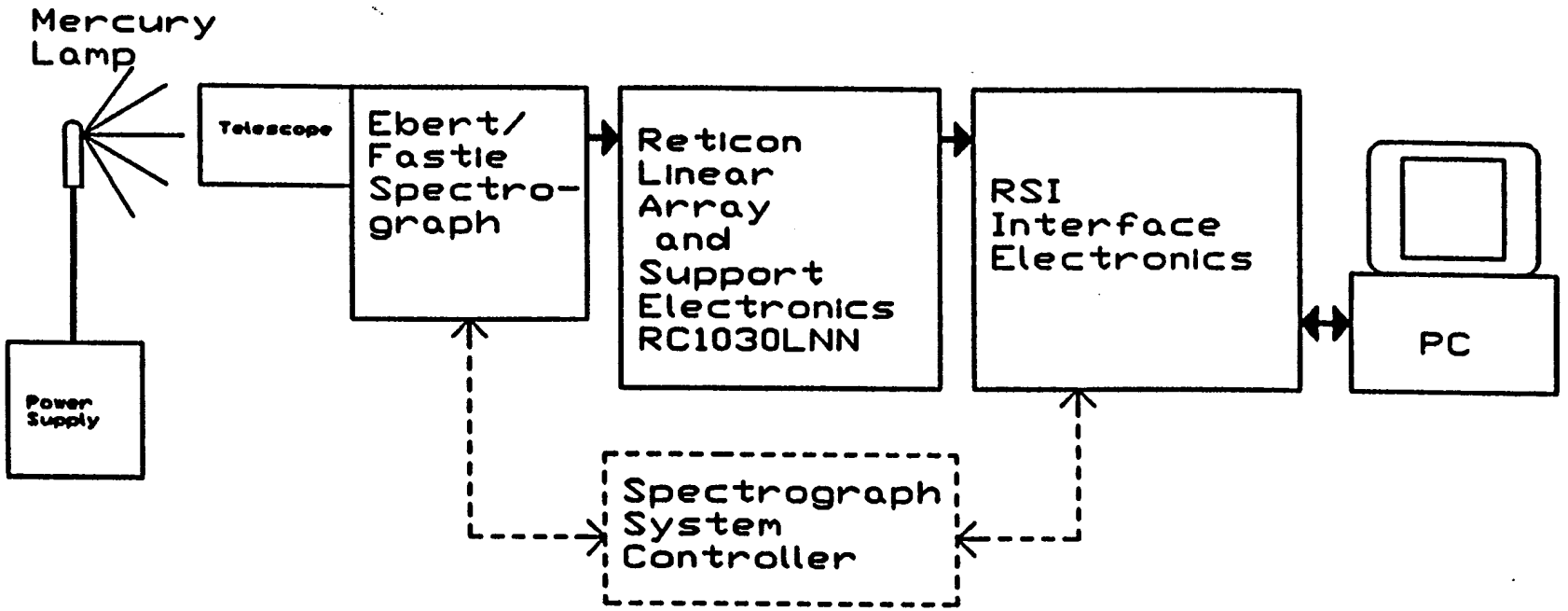

Figure 1 Linear Array Detector System and Test Setup

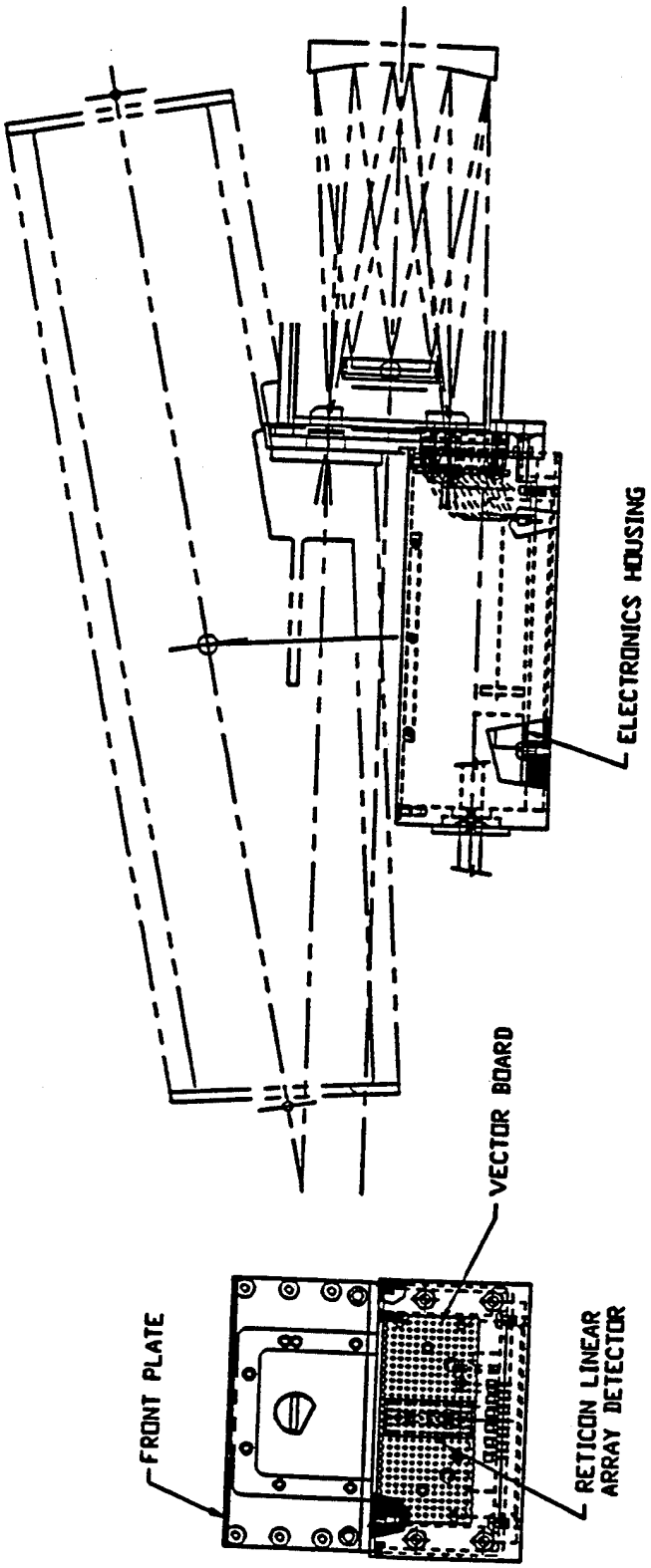

Figure 2 Linear Array Detector Spectrograph Diagram

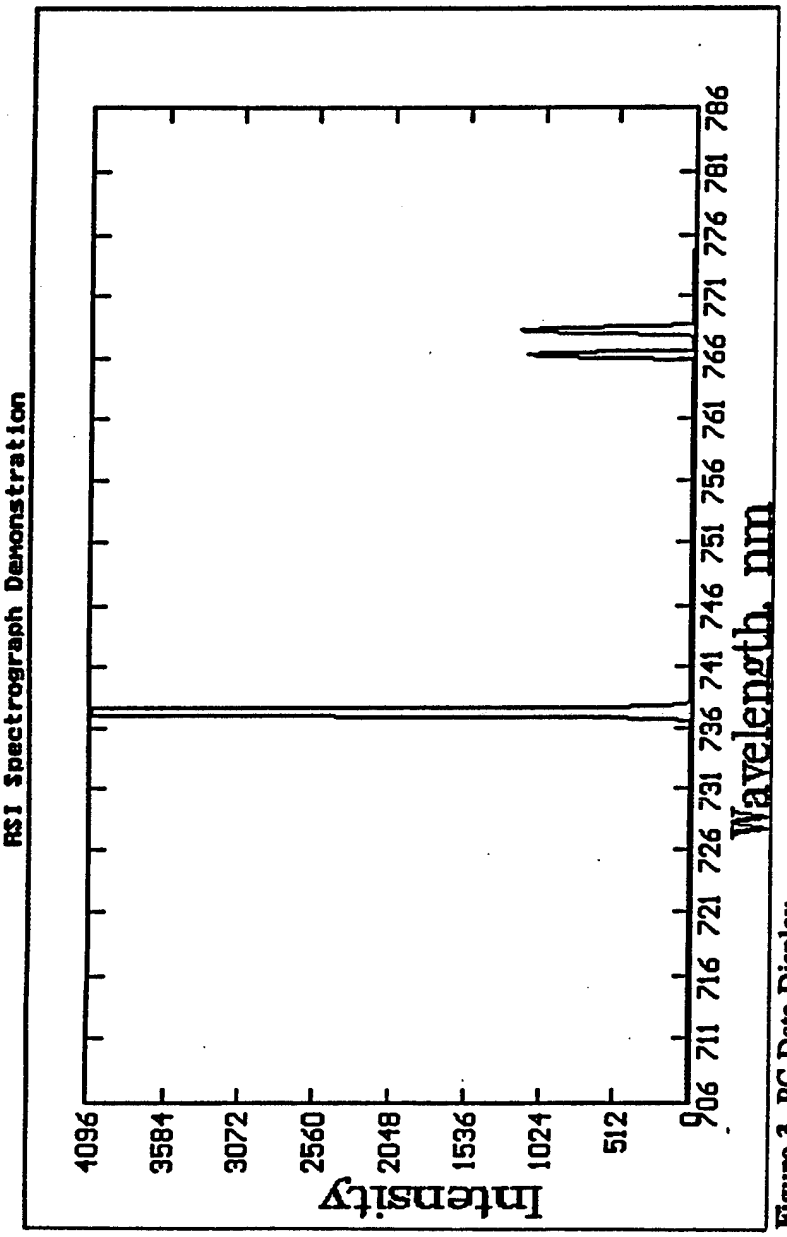

Figure 3 PC Data Display

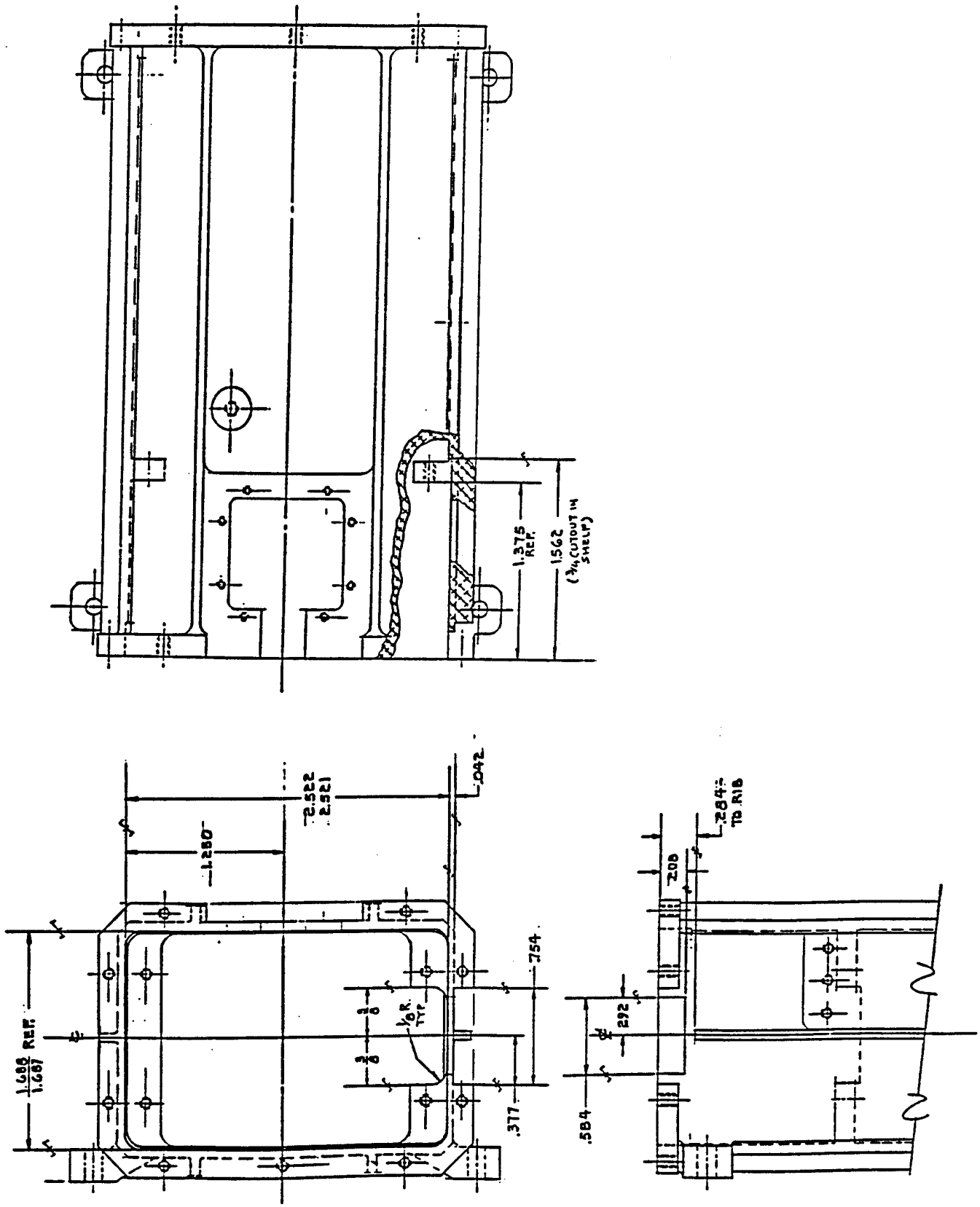

Figure 4 Housing Modifications for Reticon Mounting

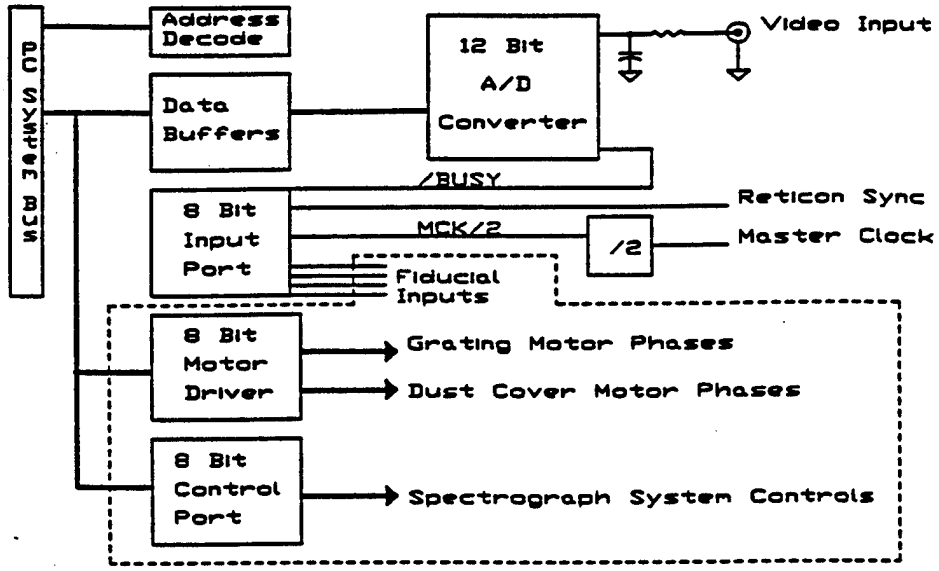

Figure 5 Linear Array Interface Electronics Block Diagram

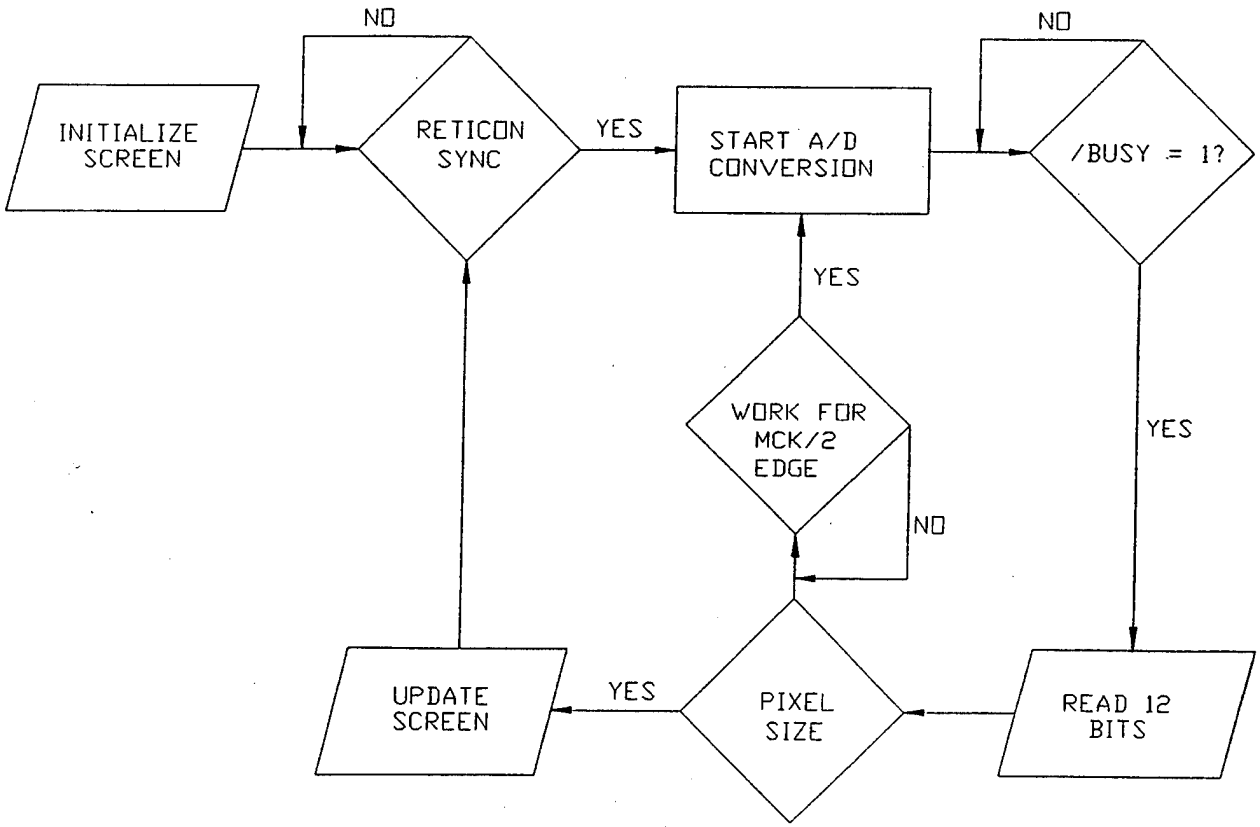

Figure 6. Reticon Data Collection Software Flow Chart

(blank)

Appendix B
AURA, an Experiment to Measure Ultraviolet Radiation of the Earth's Atmosphere from Space

Michael E. Gangl, John H. Middlestadt
Research Support Instruments, Inc.
10610 Beaver Dam Road
Hunt Valley, MD 21030
Tele: (410)785-6250, FAX: (410)785-1228

Richard W. Eastes
Phillips Laboratory
Ionospheric Modeling & Remote Sensing Branch
Ionospheric Physics Division
Hanscom AFB, MA 01731-5000
Tele: (617)377-2625, FAX: (617)377-7091

ABSTRACT

The design of the Atmospheric Ultraviolet Radiance Analyzer (AURA) is presented. The goal of AURA is to provide global measurements of the ultraviolet emissions ($\sim$115 nm to $\sim$175 nm) from the Earth's atmosphere, furnishing both spectra and images. AURA is expected to fly in a near circular, high inclination angle orbit.

AURA is designed to produce measurements sufficiently sensitive to observe relatively weak emissions from the tropical arcs and from the aurora, and to provide superb signal-to-noise measurements of the day airglow. The measurements will provide atmospheric background emissions data, and can be used to test current remote sensing techniques for measuring various physical characteristics of the ionosphere such as electron density. The AURA instrument will provide two channels of UV observation, each based on a 1/8 M Ebert-Fastie spectrometer mated to a telescope with a scanning mirror. Both can independently provide data in any one of three observational modes. Each channel can either produce images (at any desired wavelength in the range observed), spectra, or photometer mode observations. The scan mirrors and grating angles will be precisely controlled by stepper motors and will use optical fiducials to determine exact positions. When imaging, both channels can be spatially aligned to view the same area simultaneously. The 180° field-of-regard of each instrument is independent in the direction across the orbital plane, allowing for increased flexibility in the spectrometer or photometer mode observations. Thus, during such observations, the two channels can provide simultaneous information about different spatial areas. The angular field-of-view of these measurements will be approximately 1.6° by 0.2°. In conjunction with orbital altitudes anticipated to range from 700 to 1000 km, these design characteristics will result in higher spatial resolution than previous obtained with other auroral imaging instruments.

1.0 Introduction

While most UV auroral imagery from spacecraft (EXOS-A, DE, HILAT, and EXOS-D) has been at one wavelength or wavelength band [Hirao and Itoh, 1078; Frank, et al., 1981; Schenkel, et al., 1985; and Oguti, et al., 1990], the Aura experiment is designed to collect ultraviolet data at two wavelengths simulantaneously. Multispectral information has been collected by previous instruments such as the AIRS [Schenkel, et al. 1986] flown on the POLAR BEAR satellite or the UV imagers on the Viking satellite [Murphree and Cogger, 1988]. However, these instruments had characteristics which restricted their utility for quantitative, multispectral analysis. The Viking imager lacked the needed wavelength selectivity, and AIRS had fixed separation (24 nm) between the wavelengths observed.

Existing multispectral data have additional limitations. For example, almost all the data from the POLAR BEAR satellite are from the northern auroral latitude, and typically observed the auroral oval for only 5-6 sequential orbits. Furthermore, the sensitivity characterization of many UV imagers has been less than ideal.

AURA has been designed to provide a data set without many of the constraints of previous observations. Such information will help provide answers needed for greater quantitative use of UV imagery. For example, the data collected by AURA will aid in developing remote sensing algorithms for DOD users, and it will help extend UV remote sensing of the ionosphere to a global scale. Such remote sensing will have direct consequences for Radar, communications, and missile defense operations.

2.0 Scientific Objectives

AURA is designed to provide answers to questions remaining after the observations of previous instruments such as AIM on the HILAT satellite or AIRS on the POLAR BEAR satellite. The AIRS instrument provided observations at two UV wavelengths, but the wavelength separation was fixed at 24 nm. Since both channels were provided by the same spectrometer, simultaneous spectral and imaging observations at UV wavelengths were impossible. At any given time, all the UV observations were in the same mode and viewing direction. A combination of modes and viewing directions would provide significantly more useful information.

AURA will provide such data combinations by using two separate, almost identical instruments. By using two spectrometers, each with a telescope and independent scanning mirror, simultaneous observations at any combination of wavelengths is possible. Thus, emissions produced primarily by proton precipitation (i.e. 121.6 nm Lyman alpha) can be observed simultaneously with any of the more typical auroral emissions (eg. 130.4 nm OI or any desired portion of the N_2 Lyman-Birge-Hopfield bands).

AURA will also be capable of mixing modes of operation. This will allow, among other things, the reception of simultaneous UV spectra and images. Such flexibility in choosing the modes of observation was not available in any of the experiments discussed earlier.

Historically, uncertainty in the sensitivity calibration has been a problem for many UV observations. AURA is designed to observe stars periodically, which will allow the sensitivity

calibration to be maintained after launch. Each instrument is capable of observing anywhere in the 180 degree field-of-regard. From the expected orbit (>700 km altitude) this allows observation of UV stars without contamination by airglow emissions, and the entrance slit is small enough that individual UV stars can be observed.

One of the goals of AURA is the global observation of UV emissions from the Earth's atmosphere. The ability to collect global data is primarily dependent on the spacecraft, and a data recorder and sufficient power for extended periods of operation are thus necessary.

The global observation provided by the AURA design will facilitate the study of several interesting issues. For example, the latitudinal variation of the day airglow signal provides information about neutral density variations, information which is useful for analysis of auroral images. Another region of interest is near the equator where the tropical airglow arcs are seen at night. The absolute brightness of emission from these arcs (predominately oxygen emissions such as 130.4 nm and 135.6 nm) give an indication of the ionospheric electron density. The spatial variations are sensitive to equatorial electric fields and neutral winds in the ionosphere. AURA should also be capable of observing depletions which sometimes occur in the tropical arcs. The production mechanism for these depletions, which extend north to south across the arcs, is not well-understood. However, it is known that these depletions produce scintillations on radio transmissions through them, and can cause communications problems. AURA is expected to add to our understanding of this and other atmospheric phenomena.

3.0 System Configuration

The orbit planned for the AURA experiment is between 700 and 1000 km altitude with a near-90° inclination. Figure 1 illustrates the two instruments with the electronic boxes and the Ground Support Equipment. In-flight, the two instruments will be mounted to spatially scan perpendicular to the spacecraft velocity vector. The experiment is designed for a minimum 3 year lifetime, and is anticipated to fly on a class C satellite such as the Air Force's Space Test Experiments Platform (STEP).

Each instrument consists of a ⅛M Ebert-Fastie spectrometer with a 1.6° x 0.2° telescope, a scanning mirror assembly, and an integrated detector package. The spectral range of the instruments is 115 to 175 nm. Each instrument will have its optical axis aligned with the spacecraft velocity vector within ±0.5°. The spectral intensity is monitored using CsI Photomultiplier tubes in a photon counting mode. Desired spectral wavelength is varied by rotating a 3600 l/mm ruled grating blazed at 121.6 nm with a stepper motor. The instantaneous resolution is 2 nm. An optical fiducial provides the locating position of the grating, and removes the possibility of cumulative wavelength error from one scan to another due to motor slippage. Wavelengths are calibrated versus motor steps from the fiducial position.

The Scan Mirror Mechanism is capable of scanning ±90° from nadir, and 180° from nadir in only one direction for launch stowage. It has a step angle of 0.015°, and can scan spatially at a rate of 3°/second. Optical fiducials indicate seven different mirror angles, including nadir, both limbs, and stowed-for-launch position. A sun sensor with a controllable threshold level, in conjunction with a torque-motor-activated dark shutter ensures that the sun will not saturate the photomultiplier tube, or cause damage to the instrument optics. Each device includes an Instrument

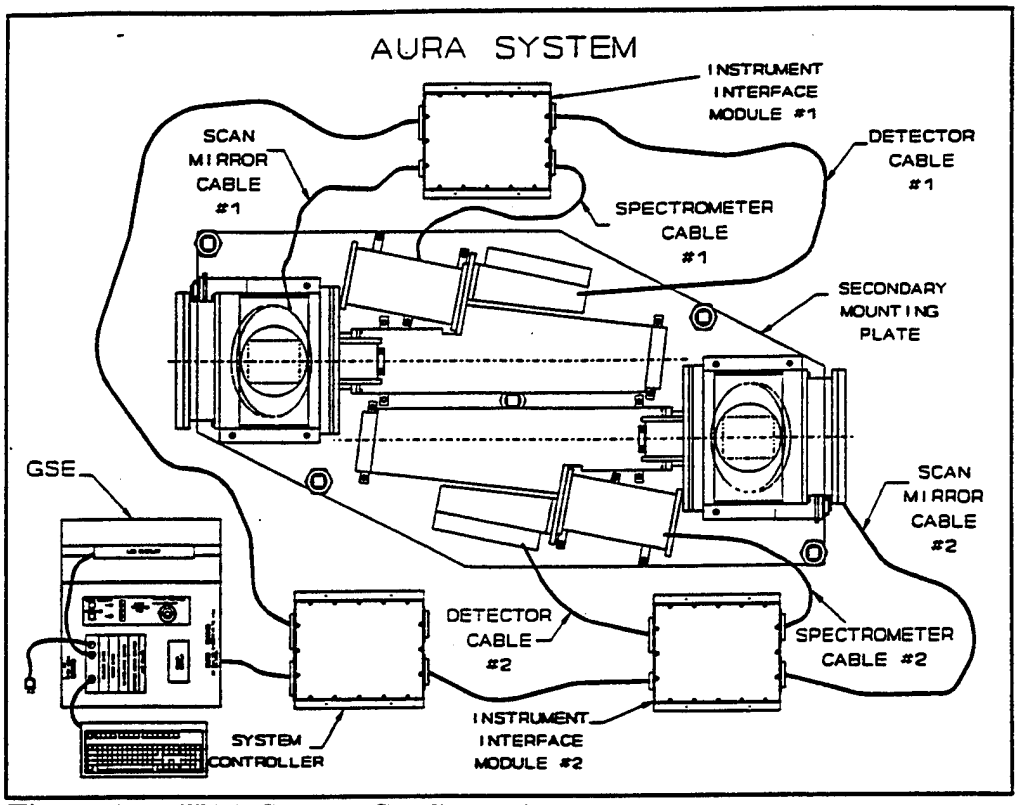

Figure 1. AURA System Configuration

Interface Module (IIM) to provide electronic control and monitoring. The experiment is operated with the System Controller, which also provides the interface to the spacecraft.

The instantaneous ground view is determined from the 1.6° x 0.2° field-of-view and the spacecraft altitude. If the AURA experiment orbits at a 700 km altitude, then the instrument footprint will be 19.6 km x 2.44 km at nadir (0°) and 85.9 km x 10.7 km at limb (64.3°). Since both instruments can scan ±90°, they provide complete coincident viewing, including calibration on a single star.

The experiment is designed to operate in several different modes selectable from the ground. These modes include spectral scanning, spatial scanning, photometer mode (staring both spatially and spectrally). There is also a self test and calibration mode which includes star calibration and dark noise measurement. The two instruments operate independently, but function in the same mode. When the two instruments perform coincident imaging, they can be set to the same spectral lines, or can view different spectral bands of the same image area. Likewise, the two instruments can view different areas at identical spectral bands.

The instruments attach to the spacecraft with a secondary plate, and the mounting of each instrument will be within ±0.5°. In addition, the operating temperature range of the experiment is between -10°C and +50°C. The communication channels with the spacecraft consists of an RS-422 asynchronous command uplink, and a RS-422 synchronous data link; the AURA experiment provides the clock and sync for the synchronous link.

4.0 Instrument Design

4.1 Optics

The AURA optical layout is illustrated in Figure 2. The optics system consists of the spatial scan mirror, the telescope off-axis parabolic mirror, the entrance slit, the spherical spectrometer mirror, the spectrometer grating, the exit slit, and the detector photocathode. All reflecting surfaces are coated with aluminum and magnesium fluoride.

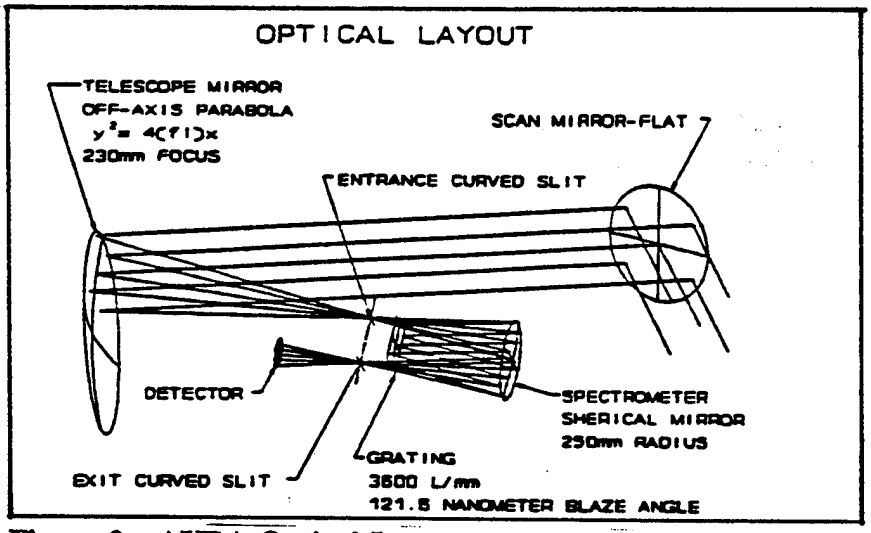

Figure 2. AURA Optical Layout.

The spatial scan mechanism rotates a plane mirror to provide a 180° field of regard for the instrument (i.e. the mirror can rotate from 0° to 180°, 90° being nadir). From an altitude of approximately 700 km, viewing angles below 21° and above 159° exclude the earth and its atmosphere, and are thus used to observe stars for instrument calibration. If a higher altitude is specified, smaller angles can be used for calibration. For example, at 1000 km, the Earth's limiting angles would be 30° and 150°.

Light from the plane spatial scan mirror is reflected to the telescope mirror, an off-axis parabola with a 230 mm focal length. The telescope then focuses the light on the entrance slit of the Ebert-Fastie spectrometer, where the entrance slit defines the instantaneous field-of-view of the instrument to be 1.6° by 0.2°, at 2 nm resolution. The field-of-view in the cross track direction will change if the spectral resolution (and slit width) are changed. The ⅛M, f/5 Ebert-Fastie spectrometer will use a 60 mm x 36 mm zero-dur mirror with a focal length of 125 mm and a replicated grating ruled at 3600 l/mm and blazed at 121.6 nm. This grating gives the spectrometer 2.15 nm/mm dispersion. A size 8 stepper motor will rotate the grating to provide wavelength scans of the 115 nm to 175 nm emissions in the field-of-view. The entrance and exit slits are curved with a width of 0.232 mm (at 2 nm resolution) and a height of 6.0 mm. This height is sufficiently less than the effective photocathode diameter of the Photomultiplier tube (9.525 mm) to avoid light loss.

4.2 Scan Mirror Mechanism

The scan mirror mechanism shown in Figure 3 provides the drive and control of the scan mirror. A 15° stepper motor, coupled with a gear reduction, rotates the scan mirror. The stepper motor will rotate the mirror through 90° in 30 seconds. Dual gear reductions are required to obtain precise scan mirror positioning and to reduce input torque. A conventional gear train of 1:12 coupled with a harmonic drive reduction of 1:80 provides a total gear reduction of 1:960. The harmonic drive operates with zero backlash, while the precision gears in the conventional gear box are designed for minimal backlash.

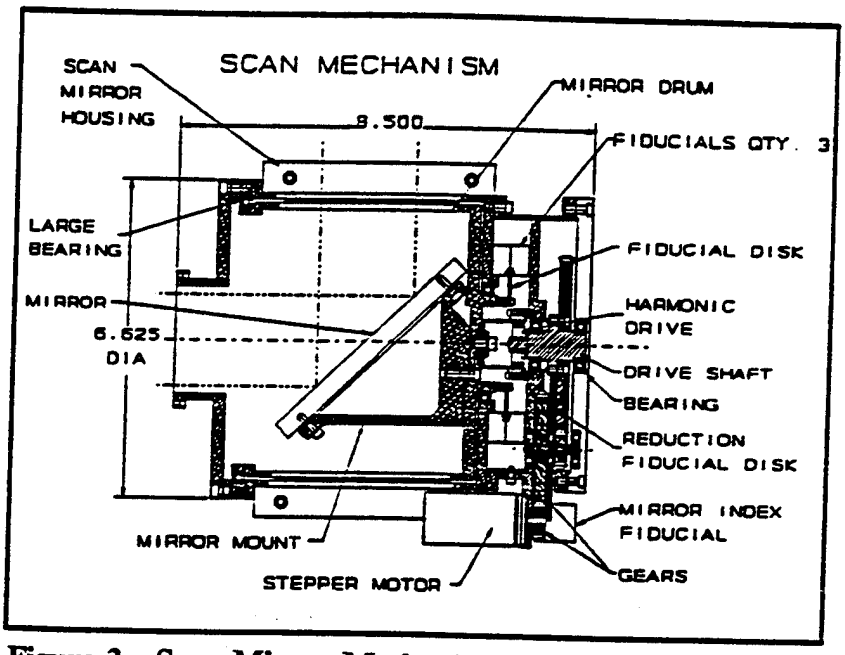

Figure 3. Scan Mirror Mechanism

The scan mirror is housed in the mirror drum and rotates on precision bearings, providing extremely accurate motion with low driving friction, and a positioning accuracy is 0.015°. As shown in Figure 4, the scan mirror rotates over the 180° field-of-view for spatial scanning, and also rotates an additional 90° to stow the optics during launch.

The scan mirror housing is a lightweight aluminum structure that attaches to the telescope, and is mounted and aligned to the secondary plate. The sun sensor is bolted to the scan mirror housing, and has a 45° field-of-view directed through the rotating scan mirror.

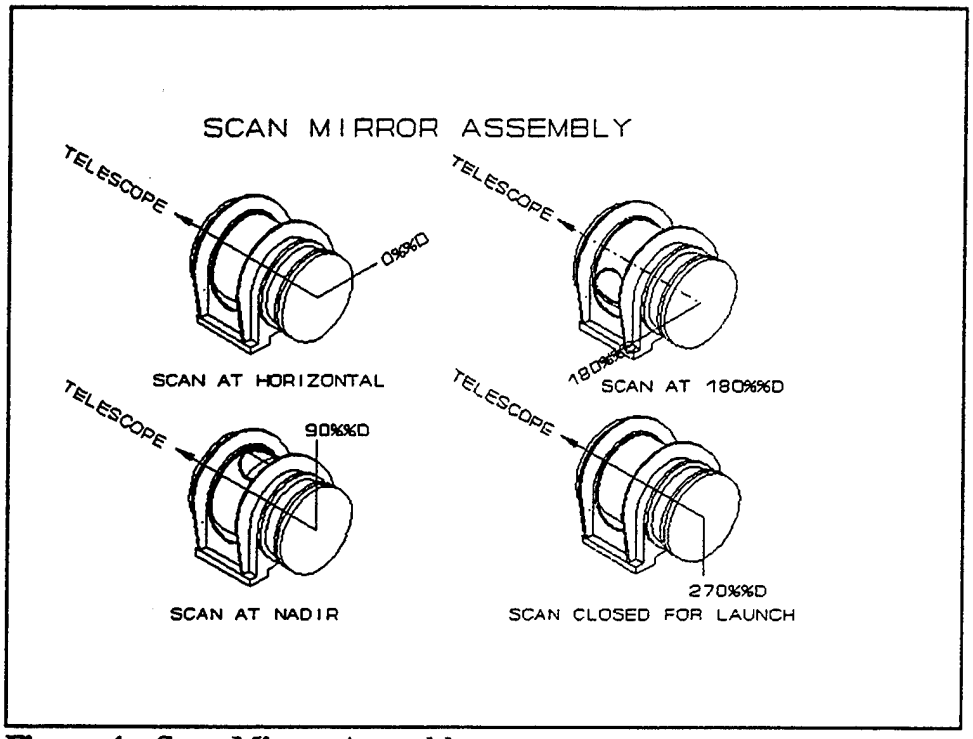

Figure 4. Scan Mirror Assembly

The mirror viewing angle is determined with the use of the fiducial system depicted in Figure 5. It consists of a single light-emitting diode (LED) with a phototransistor set switched by a rotating disk with a hole. The first gear train ratio of 1:4, and a second set of three LED/phototransistor sets referenced to the mirror rotation. The first single fiducial provides an indexing signal for every 96 motor steps. The set of three fiducials at the mirror provide seven different mirror viewing angles, including nadir, both limbs, both horizontals.

4.3 Telescope

The telescope mirror is housed within a structure by the mirror mounting as shown in Figure 6. The telescope also contains light baffling for stray light reduction. The mirror is an off-axis parabola with a 230 mm focal length, while the telescope housing is made of weight-relieved aluminum with mounting flanges for the scan mirror mechanism and the spectrometer. The housing is mounted with extension feet to the secondary plate.

4.4 Spectrometer

The focal length of the Ebert-Fastie mirror is 125 mm. As mentioned previously, the grating is blazed at 121.6 nm with a 3600 l/mm ruling and a 28 mm x 24 mm area. A stepper-motor-driven cam activates a slide mechanism that provides the 10° grating rotation. A cam rotation of 330° (rise) provides the 10° of grating motion. The other 30° is taken by the flyback of the grating to the starting angle, and a fiducial indicates when the starting position is reached.

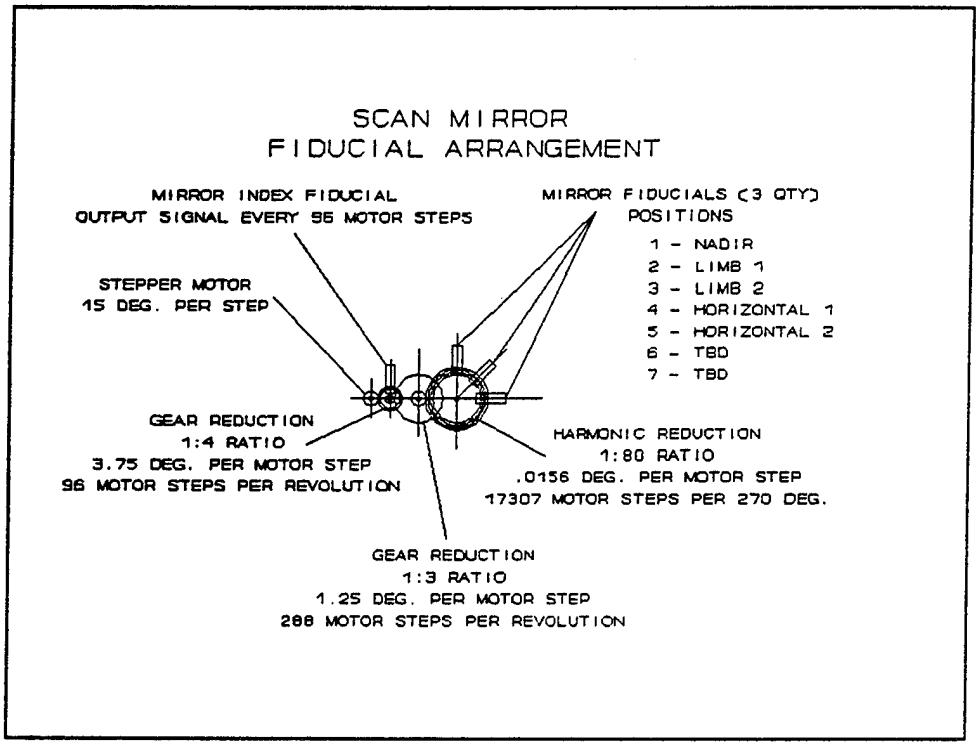

Figure 5. Fiducial System for Scan Mirror Mechanism.

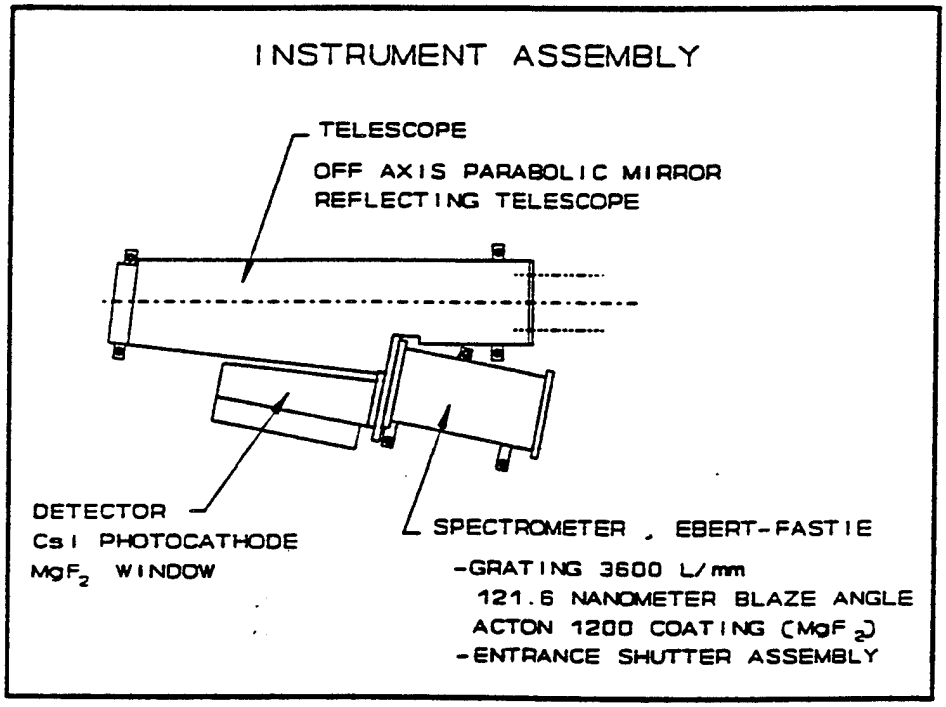

Figure 6. Instrument Assembly. Includes telescope, spectrograph, and integrated detector.

The entrance and exit slits are curved with a height of 6.0 mm and width of 0.232 mm. The dark shutter is a guillotine device located on the inside of the spectrometer, and blocks the light path upon command. The shutter is used in conjunction with the sun sensor to protect the optics and the Photomultiplier tube.

The spectrometer housing is precision machine cast, black anodized aluminum. The housing is designed with flanges to provide mounting to the telescope. Flange mounts are also provided for mounting of the detector housing. In addition, extension feet mount the housing to the secondary plate.

4.5 Detector

The integrated detector and electronics are mounted in an aluminum housing which bolts to the spectrometer at the exit slit. The detector package consists of a CsI Photomultiplier tube with a high voltage section and pulse amplifier and discriminator (PAD) electronics. The tube is operated in a photon counting mode.

4.6 Secondary Mounting Plate

The secondary mounting plate shown in Figure 7 provides the platform for the mounting and alignment of the two instruments. It is constructed of weight-relieved aluminum, and will mount to the spacecraft deck via five mounting locations. The mounting devices at these five locations will be used to align the AURA to within $\pm 0.5°$. They will also provide structural rigidity and heat transfer paths.

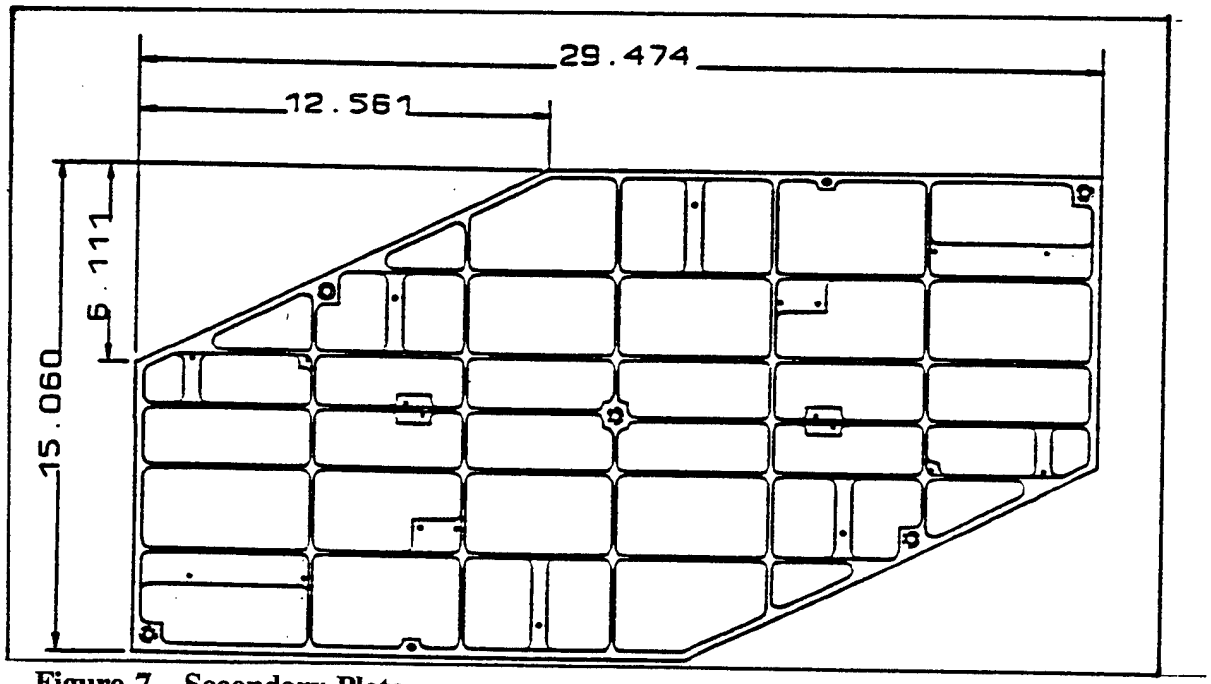

Figure 7. Secondary Plate

4.7 Manufacturing

The instruments are designed and manufactured to provide reliability and cleanliness for a three year flight, and will be purged with nitrogen after assembly and just before launch to achieve and maintain a clean optical environment.

5.0 Electronics

A block diagram of the AURA electronics is shown in Figure 8. Each instrument is equipped with an Instrument Interface Module (IIM) for direct control and monitoring of the instrument functions. The data is collected and relayed to the spacecraft by the System Controller, which also executes the various system programs depending on the operating mode selected on the ground.

The electronics are being designed with a minimum of 10K Rads(Si) with greater radiation emphasis being placed on the IIM's due to their location near, or on the outside of, the spacecraft. Electronics are being conformably coated with Conathane EN-11 to eliminate electronic component outgassing.

Each IIM consists of the drivers for the grating and the mirror stepper motors, the drive for the shutter torque motor, the digital interface for the various fiducials and integrated detector output, and the analog buffering of the solar sensor and high voltage and temperature monitors. The IIM relays all power to the instrument, and each is dedicated to an individual spectrograph.

The system controller has a Motorola 68332 microcontroller to operate the instruments in the various modes, collect data, and communicate with the spacecraft. The command and data interface to the spacecraft is achieved via RS-422 links. The commands use a 9600 Baud asynchronous link and the data from the System Controller is sent synchronously along with the clock and enable. The clock, sync, and serial data for the synchronous data link is generated by the Queued Serial Module (QSM) in the microcontroller. The system controller has two 16 bit counters, one for each instrument, and 8 bit analog-to-digital converters for all the instrument monitoring.

The system controller generates test pulses that are sent to the Integrated Detectors via the IIM's. By sending out a number of pulses on the test pulse output and reading the PMT counter, the microcontroller verifies proper operation of the detector electronics. All stepper motor phases are generated inside the microcontroller using the Time Processor Unit (TPU). The TPU also creates acceleration profiles for the stepper motor phases without using software algorithms with the CPU. This allows for ramping a larger inertia load, such as the scan mirror mechanism, to a faster speed.

A test connector with a separate UART (Universal Asynchronous Receiver/Transmitter) allows the microcontroller to be accessed by the Ground Support Equipment (GSE) computer for testing prior to launch. Just before launch, a dummy flight connector will be installed to eliminate all exposed connector pins.

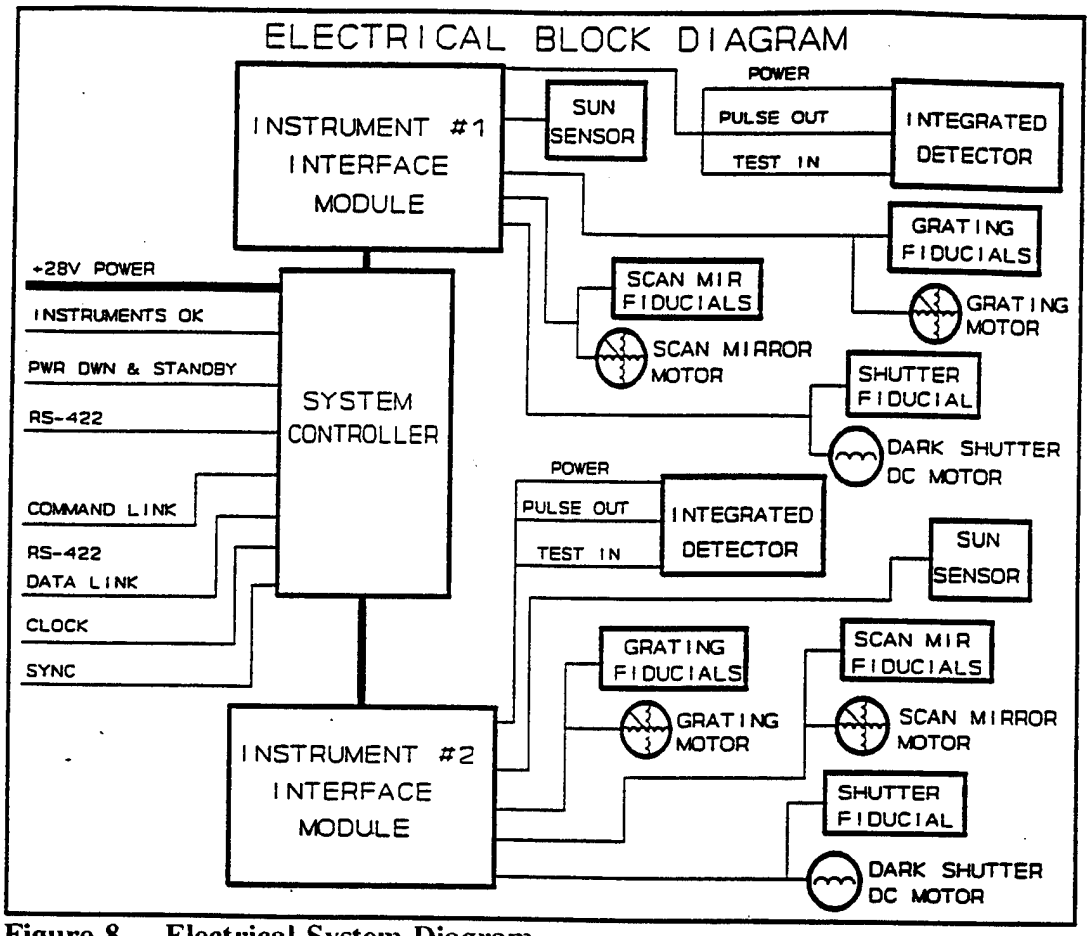

Figure 8. Electrical System Diagram.

6.0 Acknowledgements

The authors wish to thank Lieutenants Lance Pilch and Steve Clegg for their help in reviewing the document. They would also like to express their gratitude to A. Jeff Hill for supporting this paper, and Dr. R. E. Huffman for providing guidance.

7.0 References

Anger, C.D., S.K.Babey, A.Lyle Broadfoot, R.G.Brown, L.L.Cogger, R.Gattinger, J.W. Haslett, R.A.King, D.J.McEwen, J.S.Murphree, E.H.Richardson,B.R.Sandel, K.Smith, and A.Vallance Jones, An ultraviolet auroral imager for the Viking spacecraft, Geophys. Res. Lett., 14, 387-390, 1987.

Frank, L.A., J.D.Craven, K.L.Ackerson, M.R.English, R.H.Eather, and R.L.Carovillano, Global auroral imaging instrumentation for the Dynamics Explorer mission, Space Sci. Instrum., 5, 369-393, 1981.

Hiaro,K. and T.Itoh, Scientific satellite KYOKKO (EXOS-A), Solar Terr. Env. Res. in Japan, 2, 148-152, 1978.

Murphree,J.S., and L.L.Cooger, Applications of CCD detectors to UV imaging from a spinning satellite, Ultraviolet Technology II, R.E.Huffman, editor, Proc. SPIE 932, 42-49, 1988.

Oguti,T., E.Kaneda, M.Ejiri, S.Saski, A.Kadokura, T.Yamamota, K.Jayashi, R.Fujii, and K.Makita, Studies of the aurora dynamics by aurora-TV on the Akebono (EXOS-D) satellite, J.Geomag. Geoelctr., 42, 555-564, 1990.

Schenkel,F.W., B.S.Ogorzalek, J.C.Larrabee, F.J.LeBlanc, and R.E.Huffman, Ultraviolet daytime auroral and ionospheric imaging from space, Appl. Optics, 24, 3395-3405, 1985.

Schenkel, F.W., B.S.Ogorzalek, R.R.Gardner, R.A.Hutchins, R.E.Huffman, and J.C.Larrabee, Simultaneous multispectral narrow band auroral imagery from space (1150A to 6300A), Ultraviolet Technology, R.E.Huffman, editor, Proc. SPIE 687, 90-103, 1986.222

Appendix C

Summary of Evaluation of HOA1160-1

In the following evaluation we determined that the HOA1160-1 sensor was able to operate using samples of black anodize, nickel plated, polished aluminum, and stainless steel as a reflective surface. These samples resulted in a minimum output voltage of .13 v to .19 v when the phototransistor saw maximum light at a gap of .075 inch. The effect of varying the gap from .065" to .105" resulted in a negligible difference on the output voltage. Limiting the current available to the phototransistor produces an integrating effect on the fiducial signal when moving over a hole from the reflective surface. This means that the fiducial current can only be limited to the extent that it does not compromise the required fiducial transition. Random readings over all tested surfaces.of the fiducial output voltage produced variations less than .010 volts.

A hole size of .078" diameter was the minimum allowable to produce the maximum output voltage with a .075" gap from fiducial to disk. When the phototransistor current was limited to 6.4 mA, the minimum allowable hole diameter was decreased to .062". This effect can be attributed to a reduced light intensity at the edges of the LED's field-of-view. Limiting the phototransistor current with a collector resistor value greater then 1007 ohms results in an increase in collector voltage while viewing a reflective surface. Limiting the collector current also decreases the effectiveness of the fiducials with a black anodized surface.

When using a 1.8° stepper motor, the fiducial system requires the rotating disk to have a bolt circle diameter of at least 1" and holes of .062" diameter. Ringing effects were not recorded but were observed to be comparable to previous RSI built fiducial assemblies. Fiducial operation was unaffected in response when moved laterally or longitudinally off of the disk hole center when the movement was within .005".

The following are the details associated with the fiducial study.

Phase 1

EVALUATION OF HOA1160

REFLECTIVE OPTOELECTRONIC SENSOR

A. Objective :

To determine the optimum finish and gap to use with the Honeywell HOA1160.

1. Samples :

a. The following are samples to provide a variety of surfaces for evaluating the reflective requirements for the fiducial.

S1 = lathe faced ,no polishing , aluminum

S2 = lathe faced ,slight polish i.e. Scotch Brite , aluminum

S3 = polished i.e. 600 grit ,Scotch Brite ,Nevr-dull sample prepared by Mike Bullinger ; aluminum.

SB = similar finish as S3 , aluminum.

SS = electroless nickel plated surface.

BA = black anodized , aluminum

STAIN = polished stainless steel

2. Set up

a. Electrical (Figure 1)

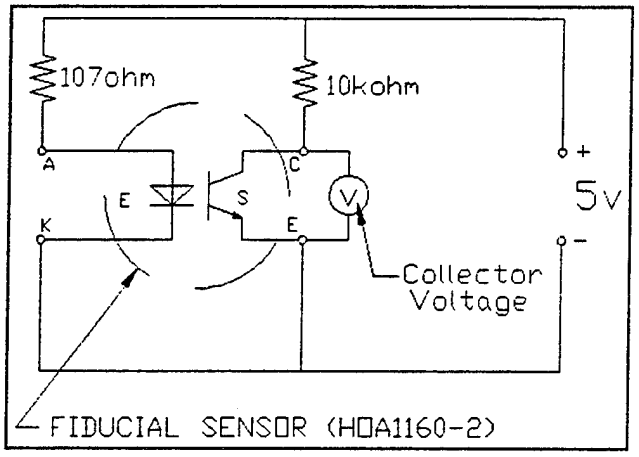

Figure 1

b. Mechanical

i. sensor mounted to the quill of a Bridgeport vertical milling machine

ii. samples clamped in vice

iii. gap measurement is from test surface to flats on face of sensor (Fig. 2)

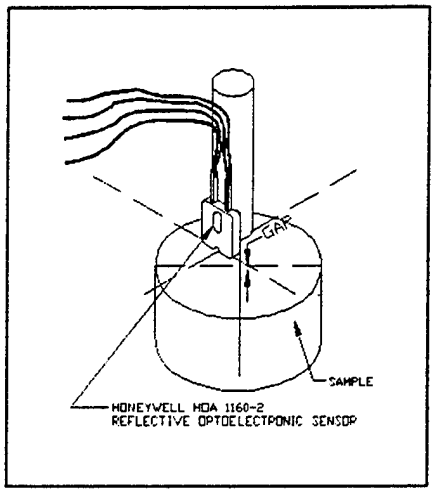

Figure 2

3. Procedure
   a. For each sample start with a gap to .025" increase by increments of .010" to .125", record sensor voltage .
   b. Randomly take 20 readings around sample at minimum setting.

4. Results
   see the following graphs
   voltage / gap (Figure 3)

   voltage / random points (Figure 4)

5. Conclusion
   a. Gap with minimum sensor voltage was consistently .075" for all surfaces.
   b. Finish samples S3,SB,SS resulted in minimum sensor voltage of less than .135" with a total variation of less than .005".
6. Design Decision
   Finish - RSI polishing process
   - start with 300 grit and progress to 600 wet/dry.
   - use Nevr-dull and\ or polishing compound and visually check against reference sample.
   - surface coated with an optical coating to protect surface finish

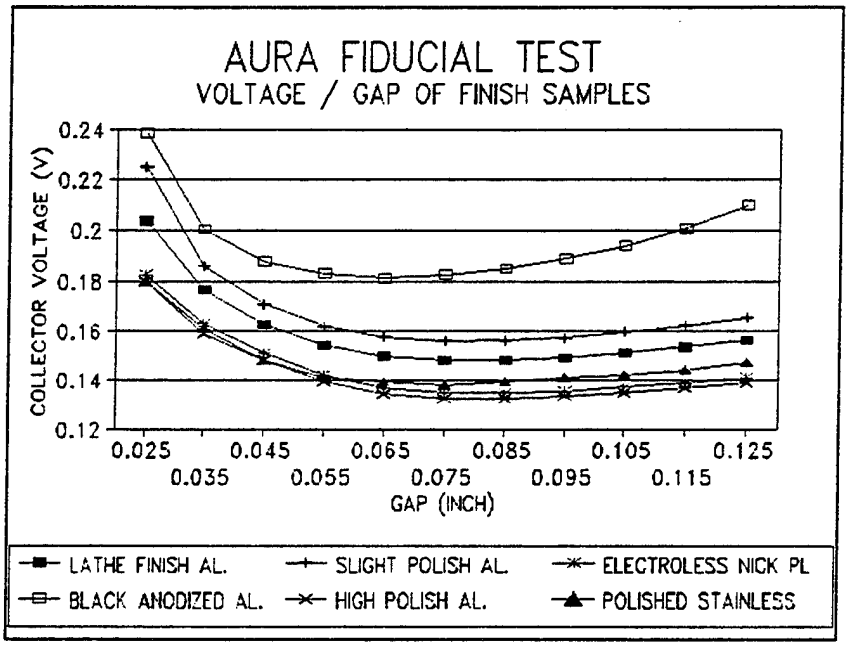

Figure 3

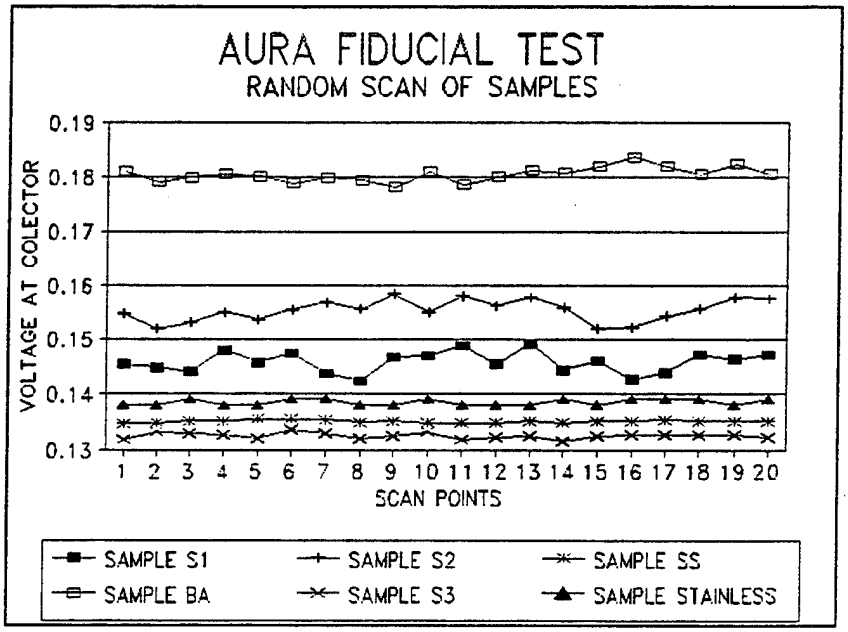

Figure 4

PHASE 2
EVALUATION OF HOA1160
REFLECTIVE OPTOELECTRONIC SENSOR

B. Objective

To determine the optimum hole size to allow a consistent triggering of a schmitt trigger

1. Sample:

a. Aluminum sheet 1/32 in. thick. drilled with the following holes :.0135", .0145" , .020" , .027" , .0291" , .040" , .052" , .060" , .070" , .078" , .086" , .096", .101" , .120" and .140". Note: minimal edge breaking both sides of sample.

b. A .060" and .078" hole was countersunk with a 120 deg. countersink from far side to a max thickness of .005". Note: the above samples have a surface finish equal to S3.

2. Set up

a. Electrical (Figure 5)

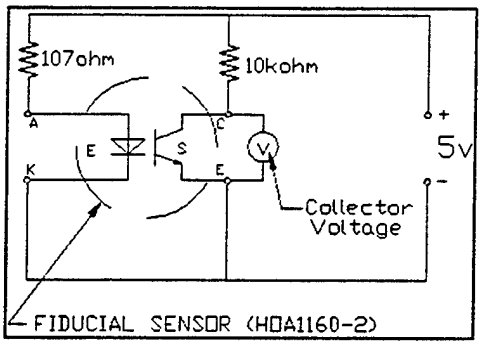

Figure 5

b. Mechanical (Figure 6)

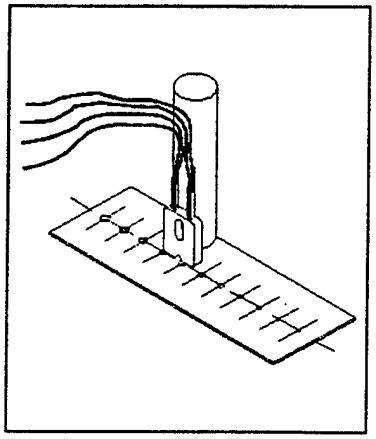

Figure 6

3. Procedure

a. Set gap to .075"

b. Find maximum volts across sensor by scanning hole to be checked in an x-y direction.

c. With the above location used as a center , move sample .050" to .100" (depending on hole size) for start of scan.

d. Voltages are recorded in increments of .002" for holes up to .060" dia. and .005" for holes over .060" dia. Step d is done for all holes listed above in samples.

4. Results

see following graphs

Hole scan .040",.050",.060" (Figure 3)
Hole scan .070",.078",.086",.096" (Figure 4)
Hole scan .101",.120",.140" (Figure 5)
Hole scan max volts/hole dia. (Figure 6)
CS .060" (Figure 7)
CS .078" (Figure 8)

5. Conclusion

At .075" gap, a .078" dia hole provides a signal which peaks out close to the input voltage without a signal extended plateau. A 0.086" dia. hole shows a plateau at the same voltage as 0.078" hole .

6. Design Decision

At 0.075" gap, a minimum hole diameter of 0.078" is necessary to reach a collector voltage approaching the input voltage. Using a gap of 0.075" will require a minimum of a 0.078" dia. hole. The holes countersunk from the far side showed little change in peak collector voltage, with some change in overall curve.

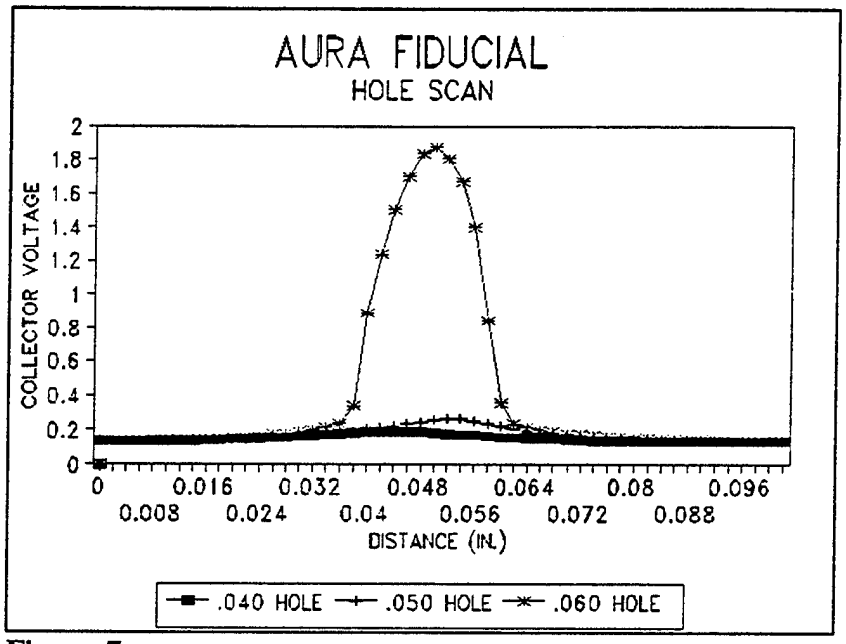

Figure 7

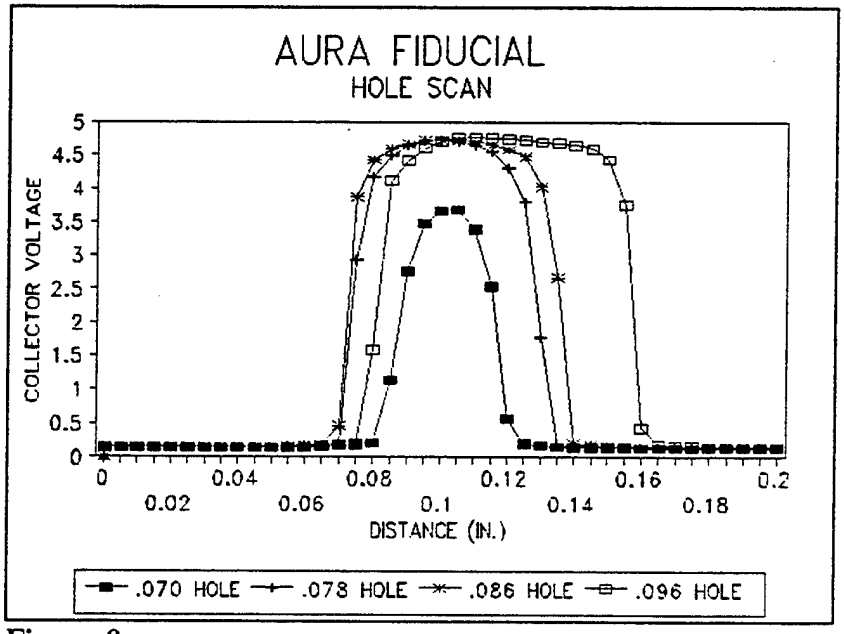

Figure 8

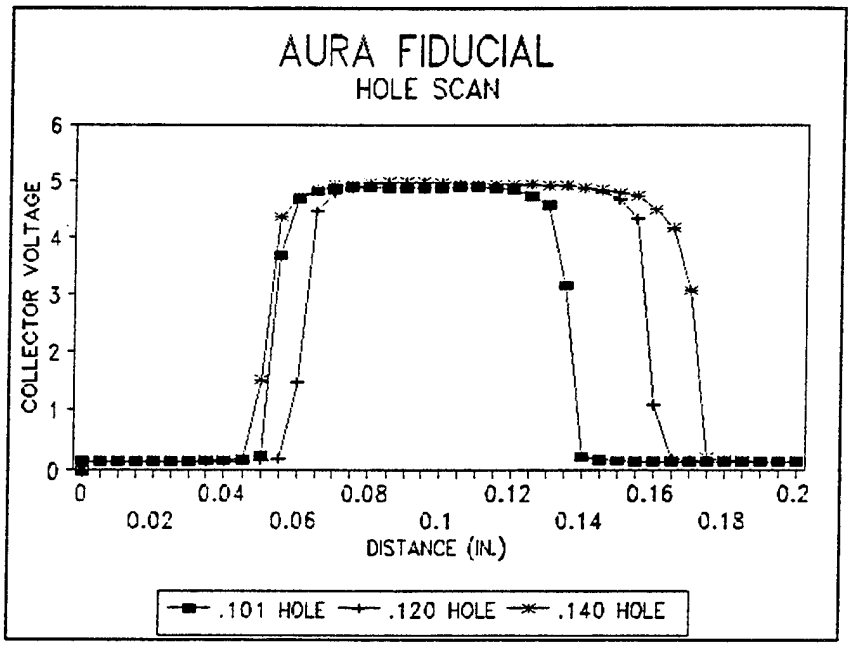

Figure 9

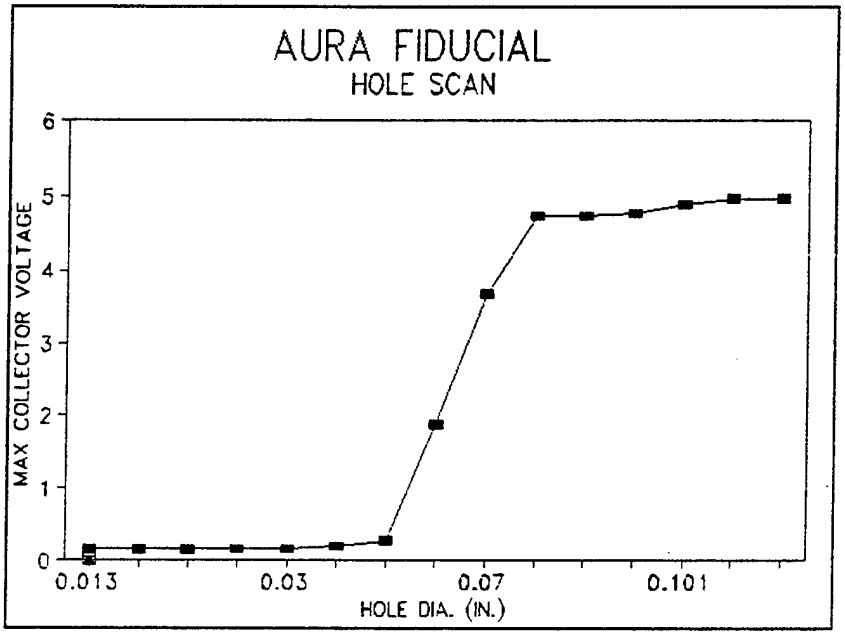

Figure 10

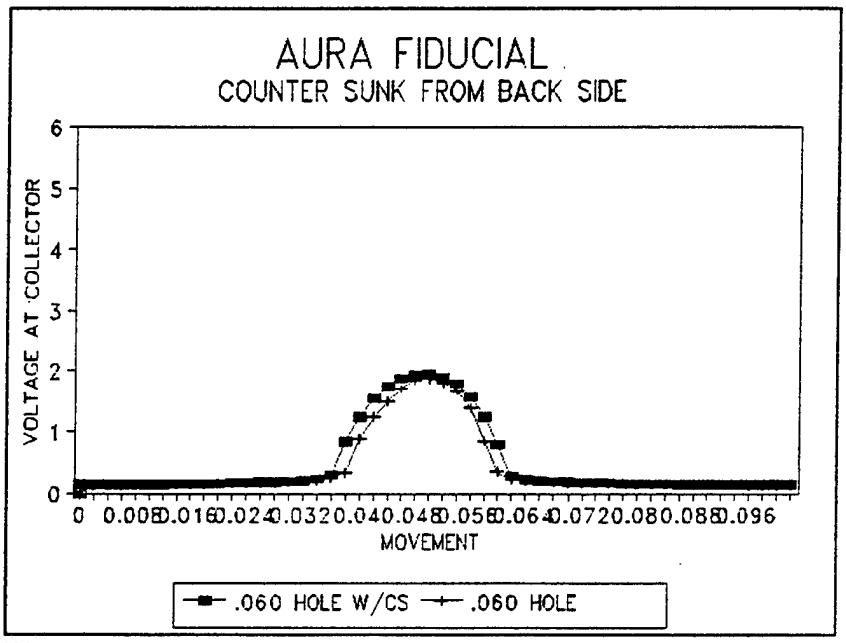

Figure 11

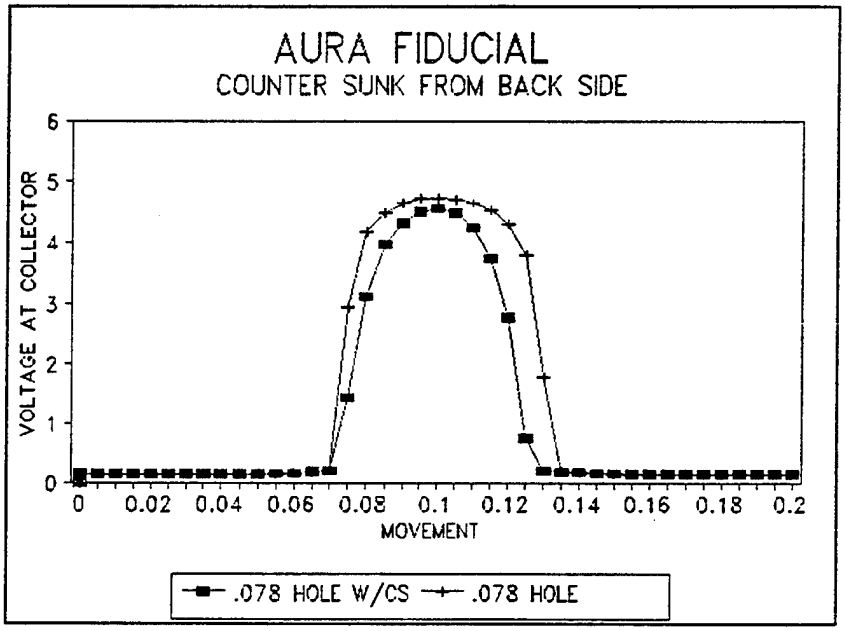

Figure 12

PHASE 3
EVALUATION OF HOA1160
REFLECTIVE OPTOELECTRONIC SENSOR
FOR USE IN AURA

C. OBJECTIVE:

To find the fiducial response to varying the current to the LED and the effects on collector voltage when scanning holes.

1. Test

a. Using a Dekabox, check response of sensor when limiting the current to the LED via the forward resistance . Resistance values to be tested are: 107 ohms to 1007 ohms in increments of 50 ohms. While using surface finish S3, take readings at both solid and open areas.

b. Rerun scans of holes .030", .040", .050", .060", and .070". Test gaps of .05", .06", and .07" using a collector resistor which minimizes overall current draw while maintaining output signal integrity.

2. Set up

a. Electrical

Replace 107 ohm resister with Dekabox in basic setup (Figure 13).

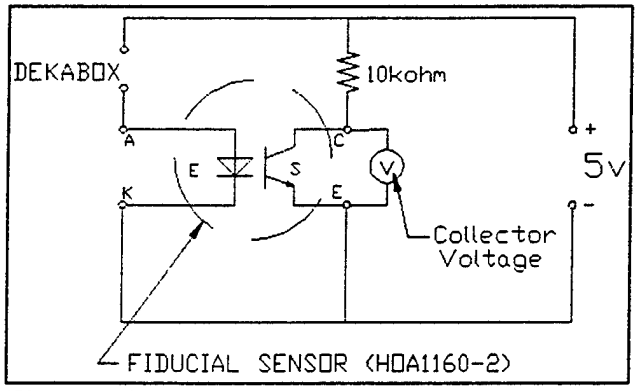

Figure 13

b. Mechanical (Figure 14)

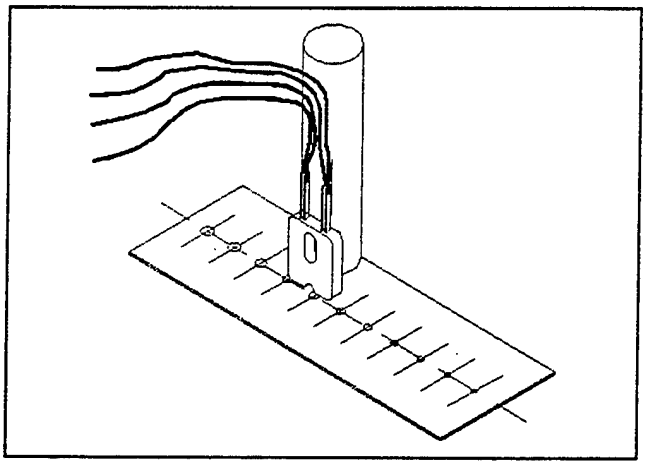

Figure 14

3. Procedure
   a. Set gap to .075" and hole diameter of .078".
   b. Position sensor over surface and test with fore mentioned resistances via Dekabox .
   c. Position sensor over opening in sample , repeat step "b".
   d. Using a resistance value determined in prior steps, scan the holes at the gaps called out above.
4. Results
   see following graphs
      Aura fiducial/ resistance variation @ 0.075" gap (Figure 15)
      Aura fiducial/ resistance variation @ 0.065" gap (Figure 16)
      Aura fiducial/ diode current limit (Figure 17)
      Aura fiducial/ gap = .05" / res. 750 ohms (Figure 18)
      Aura fiducial/ gap = .06" / res. 750 ohms (Figure 19)
      Aura fiducial/ gap = .07" / res. 750 ohms (Figure 20)

5. Conclusion
   As the current is limited to the LED with the forward resistor, the collector voltage increases gradually until the resistance is above 957 ohms. Above 957 ohms collector voltage increases drastically until it starts to plateau out at 3.54 volts / 2.357 kohms. (Figure 15). Scanning the holes shows that as current is reduced, transition points become less defined (see figure 16).
   Varying the gap effects the sharpness of the transition points as can be seen in figures 17,18 and 19. This results in a change in the transition from low to high with the transition points become more "rounded" as the gap is reduced.

6. Design decisions
   Use a 750 ohm. resistor to limit the current and still maintain a margin of .8 v less than the negative threshold. Use a gap of 0.065" which will maintain an active area having a 0.005" tolerance.

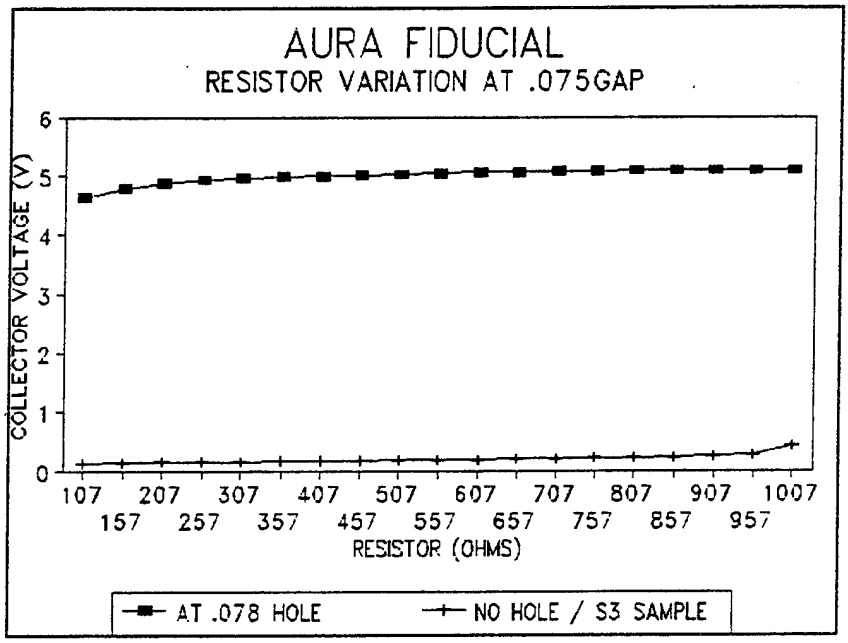

Figure 15

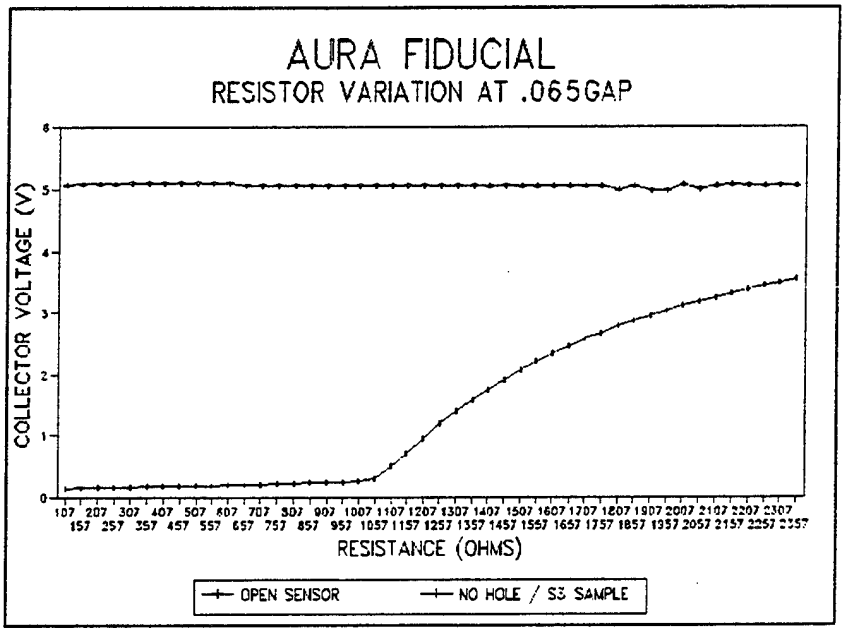

Figure 16

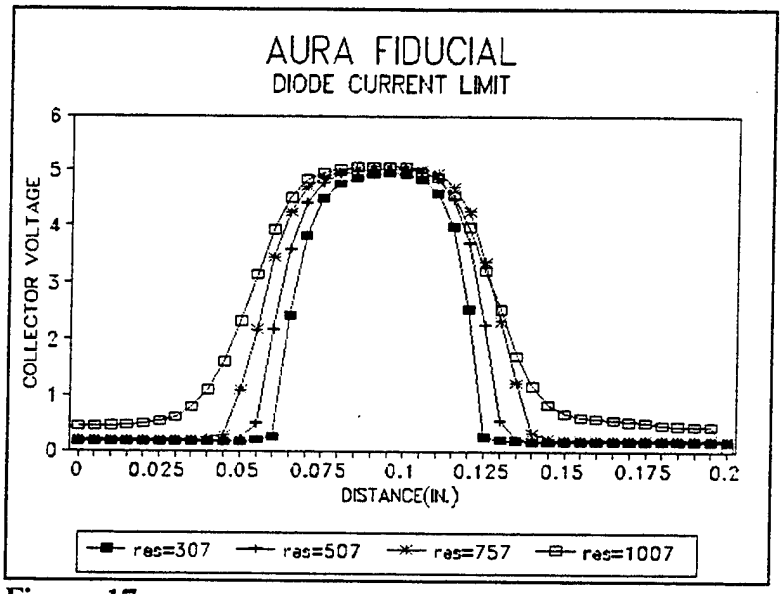

Figure 17

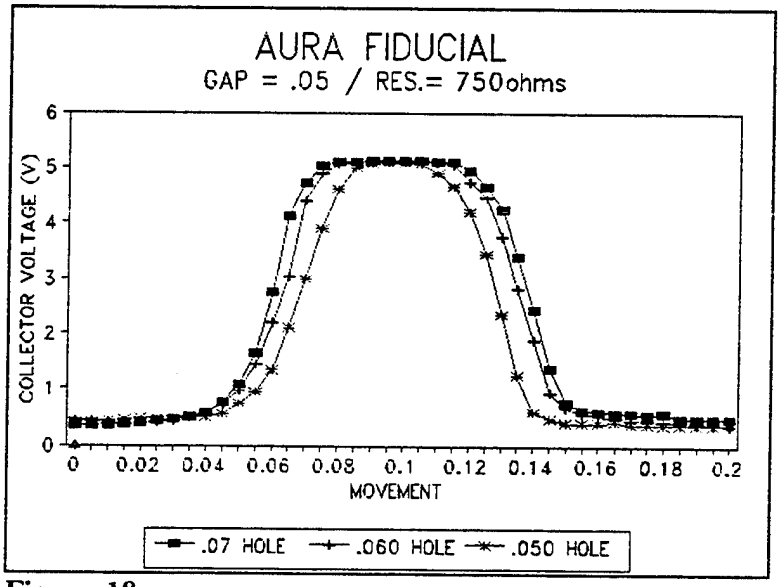

Figure 18

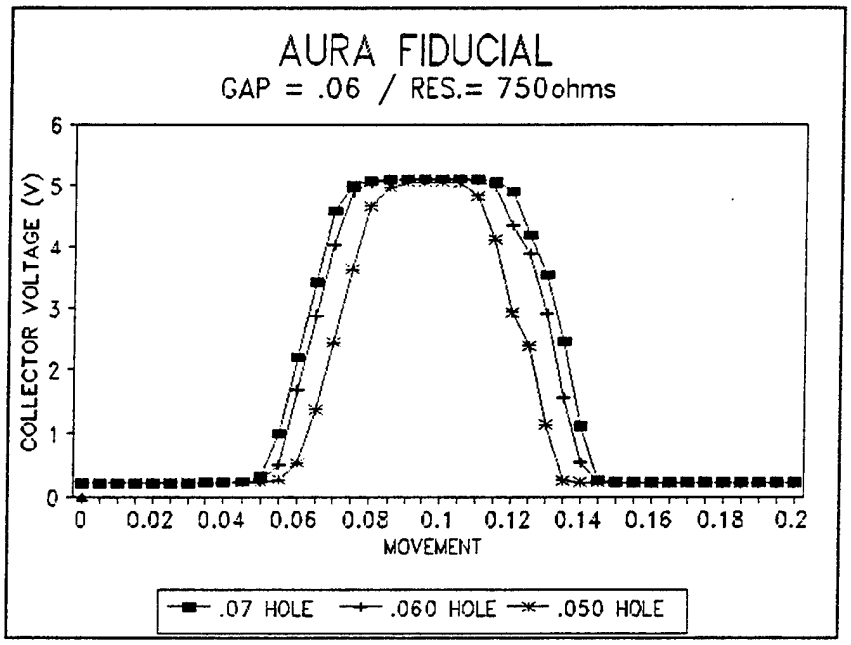

Figure 19

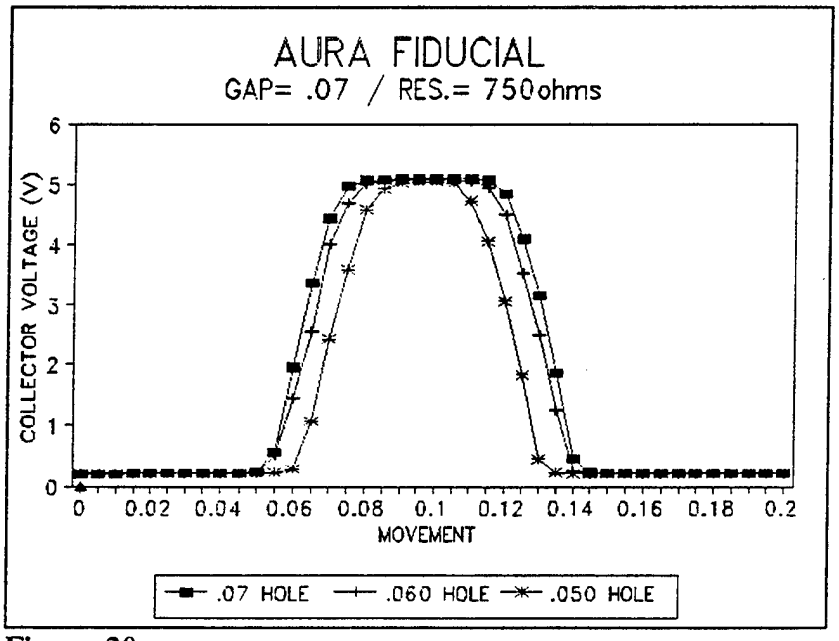

Figure 20

PHASE 4
EVALUATION OF HOA1160-2
REFLECTIVE OPTOELECTRONIC SENSOR
FOR USE IN AURA

D. Objective :
Evaluate the sensor with a 1.8 degree/step stepper motor and fiducial disc .

1. Test

a. Use an Astrosyn miniangle stepper (1.8 deg) and a fiducial disc having the following holes.

	hole pattern radius(in.)		
	.4	5	.6
h	.031	.031	.031
o	.039	.039	.039
l	.046	.046	.046
e	.052	.052	.052
		.055	.055
d	.062	.062	.062
i		.072	.072
(in.)			

2. Set up

a.Electrical

Replace Dekabox with a 750 ohm resister (Figure 21).

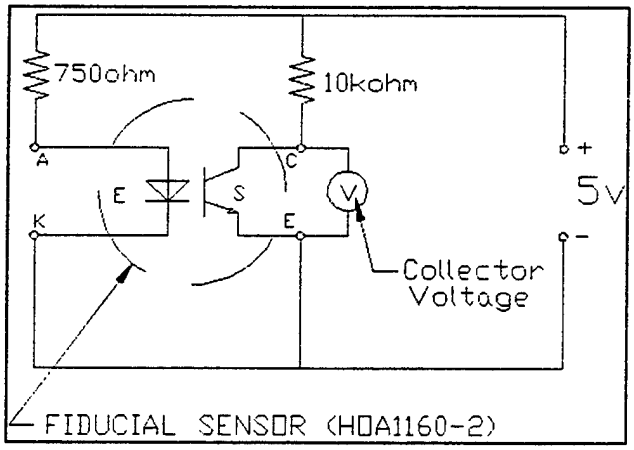

Figure 21

b. Mechanical

- Use a 1.8 deg stepper motor with a fiducial disc which is .032" thick and a diameter of 2" with the above through holes and finished to a S3 (Figure 22).
- Mount motor in vice on a vertical mill.
- Sensor is held above disc at .065" gap.
- Motor is driven by a single phase driver, Spectrometer Controller # 801-150. .

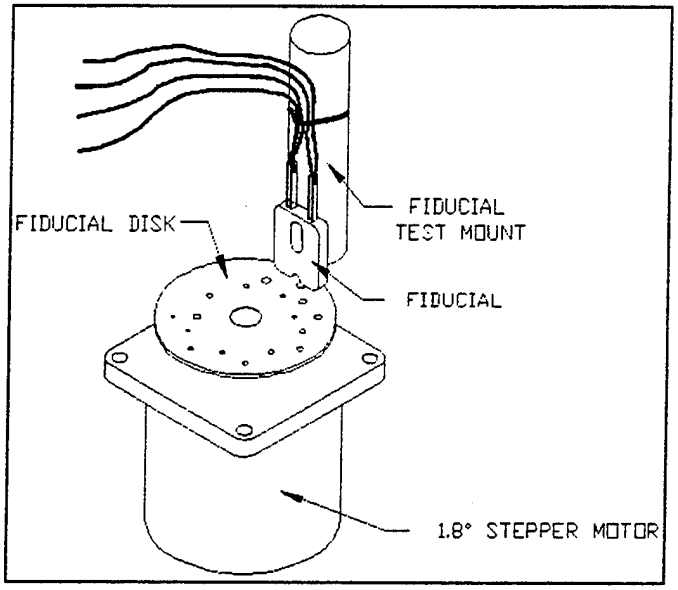

Figure 22

3. Procedure
   a. Set gap to .065"
   b. Center sensor over hole by scanning for maximum collector voltage.
   c. Single step motor 10 steps ;reverse and scan 20 steps across hole recording collector voltage at each step.
   d. Repeat steps b.and c. for all holes and hole circle diameters.

4. Results
   see following graphs
   AURA FIDUCIAL .031 DIA. HOLE (Figure 23)
   AURA FIDUCIAL .039 DIA. HOLE (Figure 24)
   AURA FIDUCIAL .046 DIA. HOLE (Figure 25)
   AURA FIDUCIAL .052 DIA. HOLE (Figure 26)
   AURA FIDUCIAL .8 BCD (Figure 27)
   AURA FIDUCIAL 1 BCD (Figure 28)
   AURA FIDUCIAL 1.2 BCD (Figure 29)

5. Conclusion

a. The .8 dia. bolt circle to have 4-5 steps high a hole of 0.031" dia. which allowed a collector voltage of 4.5 v. with no plateau.

b. The 1.0 dia. bolt circle to have 5 steps high a hole of 0.062" dia. allowed a collector voltage of 5 v with a plateau two steps .

c. The 1.2 dia. bolt circle to have 4 steps high a hole of 0.062" dia. allowed a collector voltage of 5 v with a plateau two steps.

6. Design decision

a. The index fiducial will use a 1.2 dia. bolt circle with a 0.062" dia. hole , and a 0.065" gap.

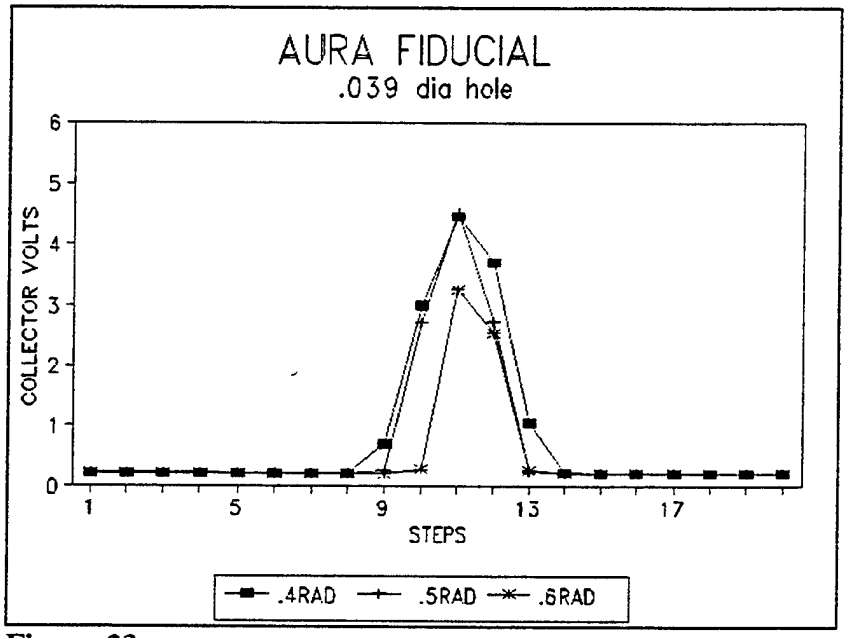

Figure 23

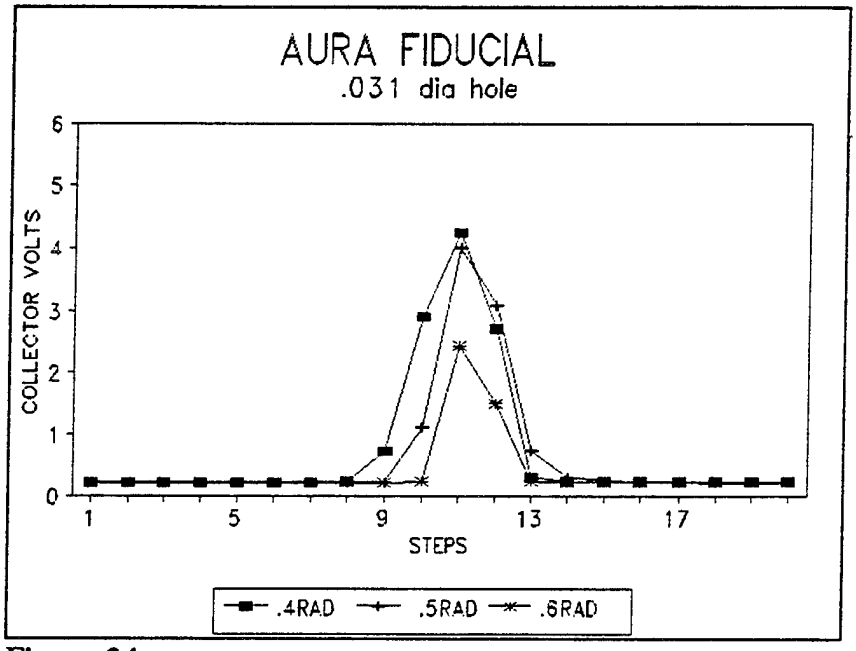

Figure 24

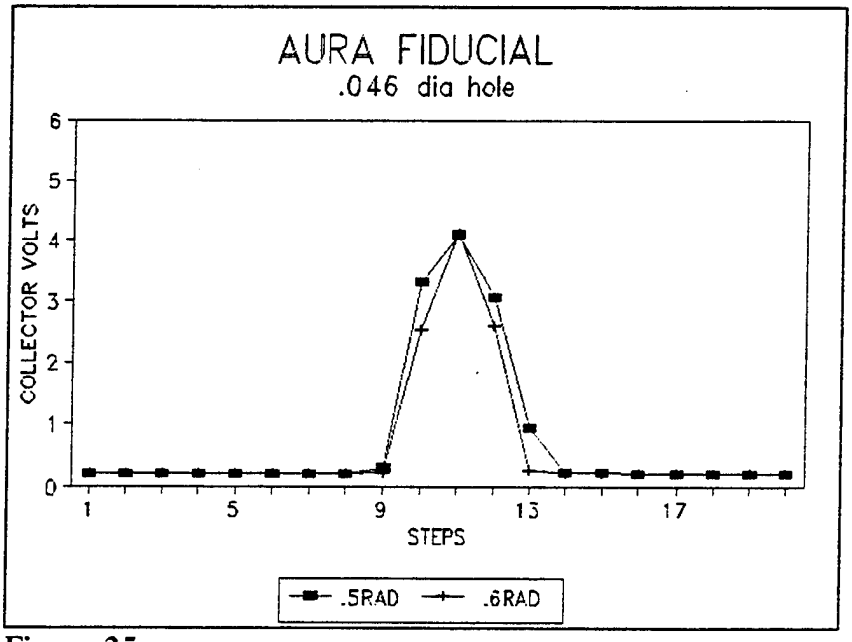

Figure 25

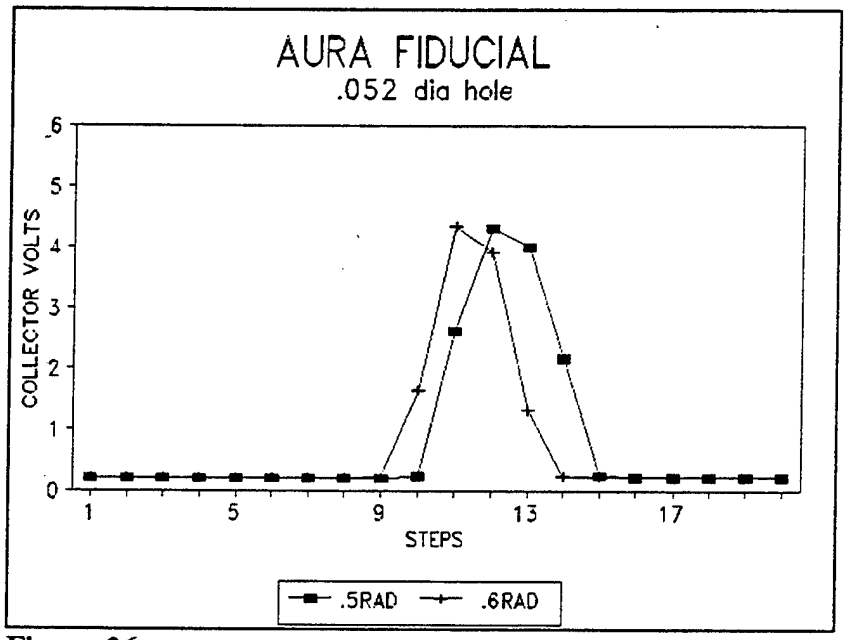

Figure 26

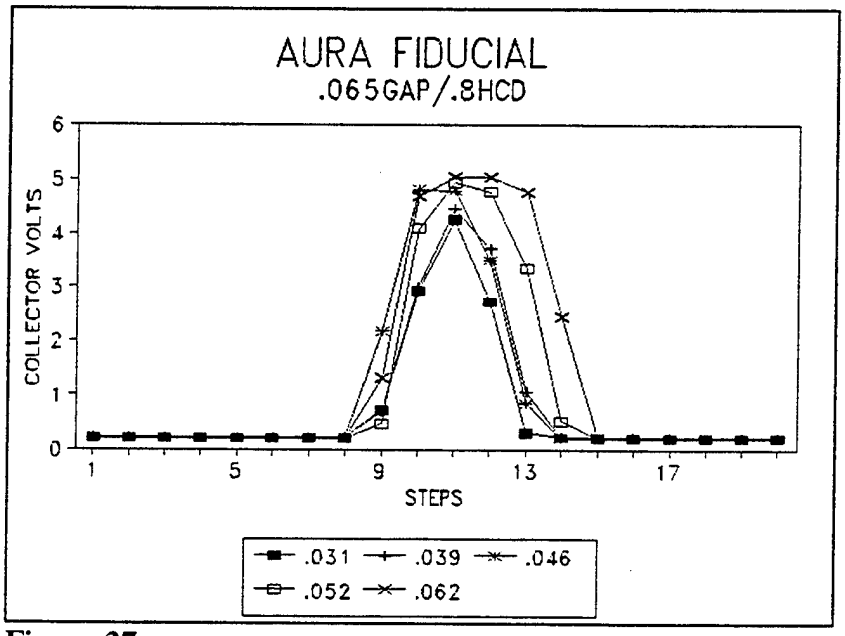

Figure 27

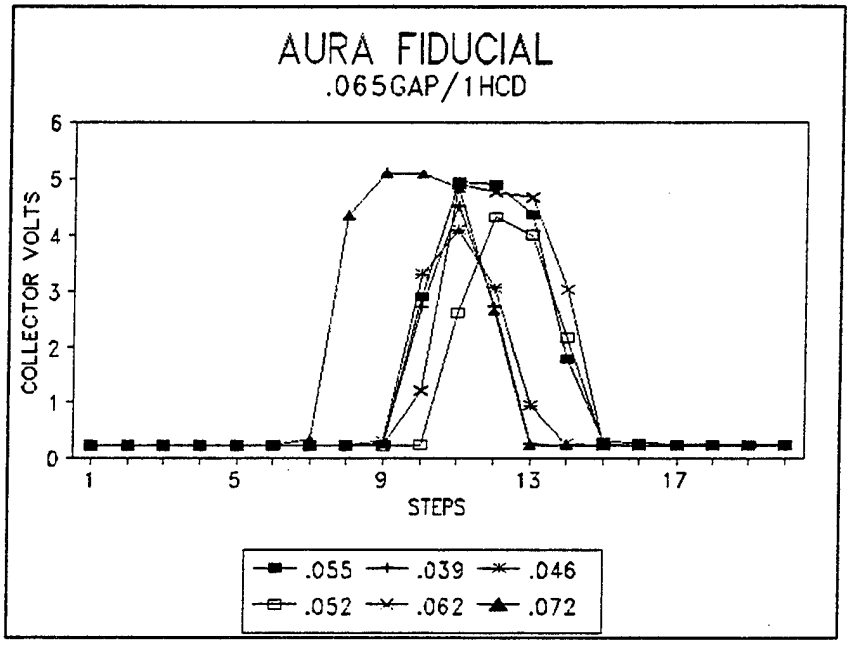

Figure 28

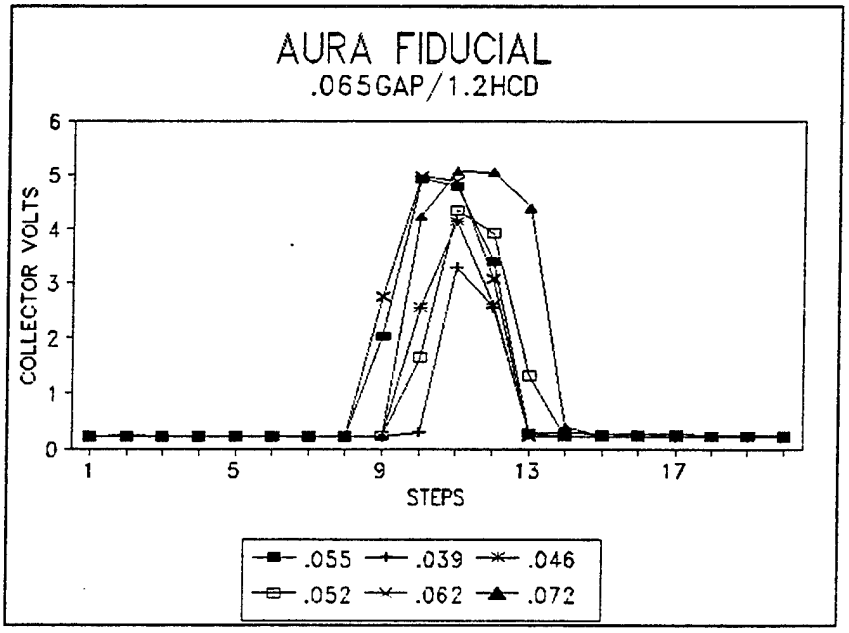

Figure 29

PHASE 5
EVALUATION OF HOA1160-2
REFLECTIVE OPTOELECTRONIC SENSOR
FOR USE IN AURA

E. Objective:
Determine effects of moving sensor off of hole center by .005" in the "X" and "Y" axis parallel to the reflecting disk surface.

1. Test
   a. Move sensor in the +X , +Y , -X , -Y , +X+Y and -X-Y direction .005" in. and scan the .062" dia. hole on the fiducial disc at the .5" and .6" hole circle radius.

2. Set up
   a. Electrical (Figure 30)

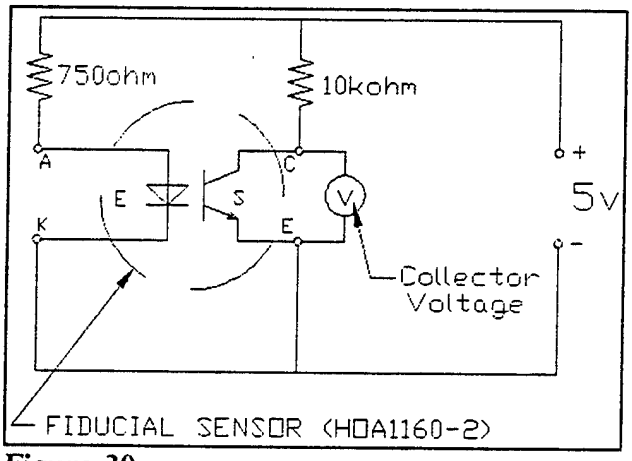

Figure 30

b. Mechanical

- Set up is shown in Figure 31.
- Orientation of off-sets is shown in Figure 32.

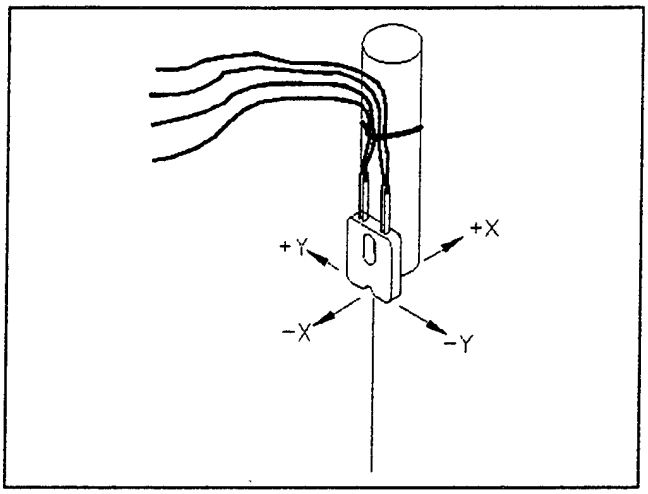

Figure 31

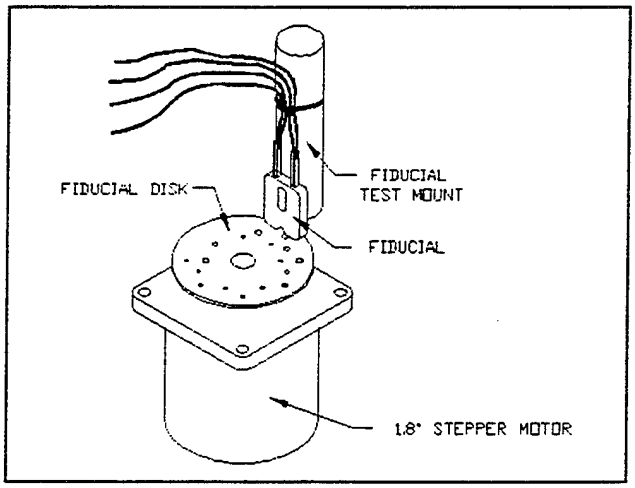

Figure 32

3. Procedure

a. find center of hole with sensor as per previous test

b. X-axis

i. move +.005" and move 10 steps away from hole. Reverse 20 steps and record collector voltage.

ii. move -.005" and repeat step scan.

c. Y-axis

i. move +.005" and move 10 steps away from hole and reverse 20 steps , record collector voltages.

ii. move -.005" and repeat step scan.

d. X / Y axes

i. move +.005" and move 10 steps away from hole and reverse ,for 20 steps and record collector voltage.

ii. move -.005" and repeat step scan.

4. Results

see following graphs

AURA FIDUCIAL .065GAP\1HCD\.062 HOLE (Figure 33)

AURA FIDUCIAL .065GAP\1.2HCD\.062 HOLE (Figure 34)

5. Conclusion

Changing the lateral position of the fiducial relative to the hole center showed no appreciable change in collector voltage position within a radial movement of .005". Moving the fiducial in X, Y, or an X-Y hypotenuse much greater can result in the fiducial "firing" at an adjacent motor step position.

6. Design criteria

0.005" is acceptable for a tolerance of fiducial positioning.

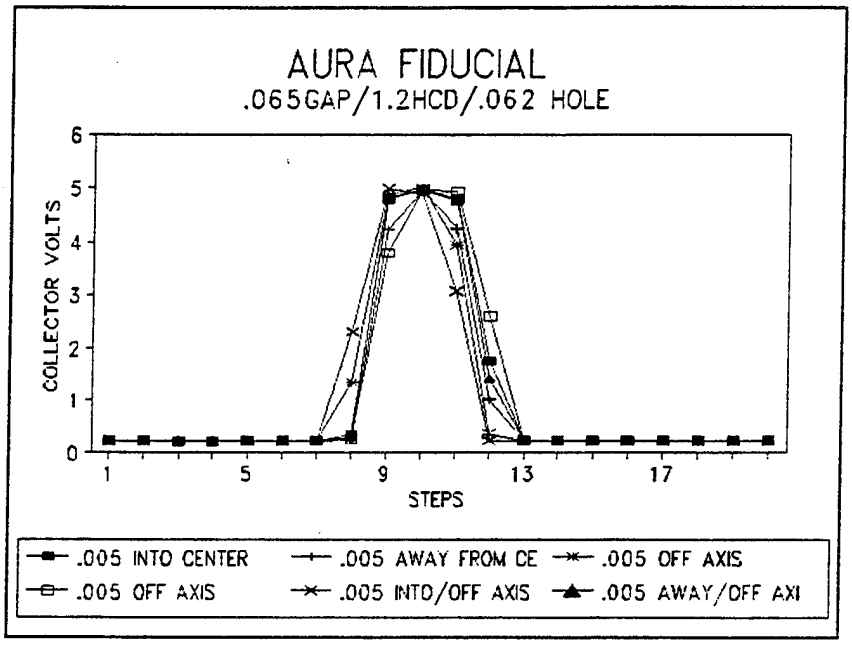

Figure 33

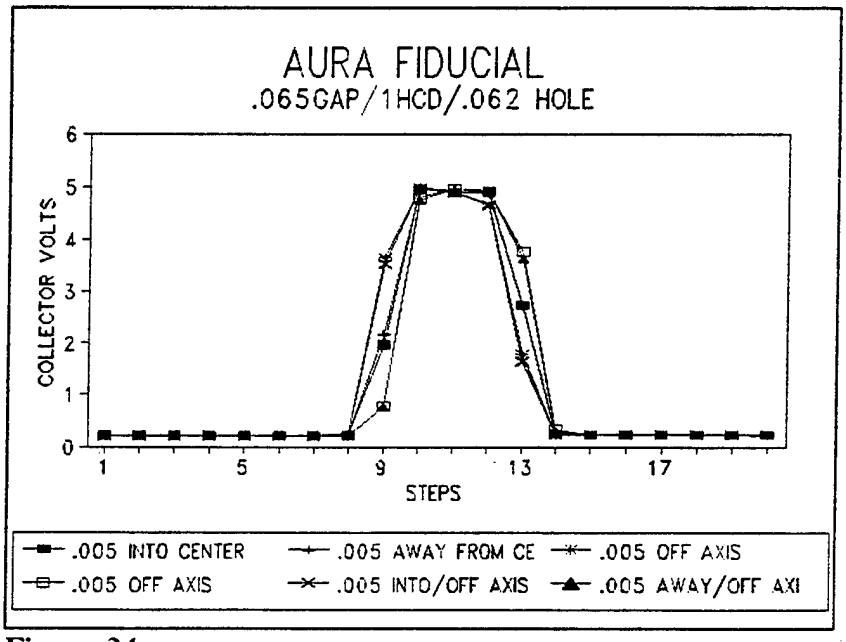

Figure 34

Appendix D

1.0 System Controller Development Work

As part of the development of the AURA program, the System Controller board required breadboard testing prior to building the flight hardware. While the baseline design created a sophisticated processing system for the minimal size and power, using the latest technology to achieve these goals meant that the new designs required thorough testing. RSI built and successfully tested a prototype version of the System Controller board. This appendix will explain how and what was performed with the prototype to ensure a compliant design.

After the inital design of the System Controller was completed, a breadboard version was built by our assembly group that consisted of sockets for the various integrated circuits and made the point-to-point connections through wirewrap. The schematic of the final design, Figures 1, 2, and 3, are included. The testing of the hardware (and associated software) proceeded in a step by step manner, starting with the 68332 microcontroller interface to the RAM and ROM and ending with the testing of the interface with peripheral devices. The following description explains the proper operation and testing methods used.

The prototype board was brought to an operational state. Upon power up, the board is configured by the micro-controller by proper setting of the processor's chip select registers to enable access to RAM, three A/Ds, PMT counts, and numerous discrete I/O pins. Additionally a test communication interface, when present, is initialized and control is passed to the resident Microtech monitor. The monitor is software code that resides in ROM on the board. When the interface is not present, the application/mission program is directly executed.

The Microtech monitor interfaces with the host PC program called the Xray Debugger via an RS-232 link. The XRAY68K Debugger monitors and controls the execution of high-level C programs or assembly-level programs in the controlled environment of the host computer. The engineer can then download test programs from the Debugger to the monitor in the computer without "burning" PROM's.

XRAY lets the user examine or modify the value of program variables using the same high-level or assembly-level terms, definitions, and structures that were defined in the original source code. XRAY employs a window-oriented user interface.

The debugger is interactive and gives complete control of the program. It executes the program while allowing access to variables, procedures, source line addresses and other program entities. XRAY's command language allows simple and complex breakpoint setting, single-stepping, and continuous variable monitoring.

The various functions of the design tested successfully with the prototype include:

1) access and execution of ROM monitor programs.

   a. Test of the communication between the X-Ray debugger in the host PC with the monitor built into the breadboard's ROM. This ran out of the ROM space only.

   b. Test of the RSI monitor (RSIMON) which programmed the ROM with the AURA parameters along with the monitor. This allowed us to load programs into RAM for further testing.

2) access to internal and external RAM. This included a memory test.

3) programmability of processor clock to 16.78MHz. The frequency was verified through the monitoring of the "clock out" pin of the microcontroller.

4) periodic interrupt clock duration of 5.005 msec. This was measured via toggling an I/O pin on the microcontroller resulting in a 10 msec clock output. The pulse length was measured between clock edges to get the 5.005 msec.

5) manipulation of discrete I/O pins.

6) tested communication interface, both command and telemetry links.

   a. *Command Link, Serial Communication Interface (SCI)*

      i. *downlink* - created software code that transmitted a "ready" message to a receiving PC with XTalk (a software program to communicate over the PC's COMM port).

      ii. *uplink* - created software code that collected an ASCII character from the PC with XTalk and relayed it to the host computer with the XRay debugger while also relaying it back to XTalk.

   b. *Telemetry Link, Queued Serial Communication Interface (QSPI)*

   The breadboard was set up as the Master QSPI while the Motorola Evaluation board was set up as the Slave QSPI. The software code created incremental words that were transmitted from Master to Slave and then were relayed to the PC with XTalk. This was the most straight forward and economical meathod of testing the telemetry link.

7) use of autovector interrupt for RS-232 communication.

8) ability to read and detect changes in A/D values. The test setup was comprised of inputing voltage levels to the channels of the analog to digital converters and reading the measured count at the host computer with the XRay debugger. Values were verified with a logic analyzer on the A/D outputs. There are three 8-bit A/D converters, each with eight

channels. On the breadboard, all eight channels of U8 are used while the least significant four channels of both U9 and U10 are used. Testing shows that the maximum error between calculated and measured count values for the input voltages was 2.5%. The tests also verified the identical gain and offset error for all the channels within an A/D package. In the flight system, each A/D IC will have its own offset adjustment for removing that error, and all channels will be calibrated through testing.

9) testing the stepper motor phase generation with the 68332 Timed Processing Unit (TPU). Using the logic analyzer on the TPU output pins, the required patterns for the scan mirror and spectrometer motors were verified. The concept is that the TPU will provide the four phases for the stepper motors inside the microcontroller, reducing the amount of periperal equipment. Also, the phase patterns and directions can be controlled through software. This provides added flexability during integration of the flight hardware. The scan mirror TPU channels were run in a bi-phase configuration while the spectrometer TPU channels were operated single phase.

A Hewlett Packard 1653b Logic Analyzer was used to verify subtasks 1,2,6,7, and 8 by direct connection to the bus and interrupt pins. A Tektronix 2230 100 MHz Digital Storage Oscilloscope was used to verify subtasks 3 and 4 by monitoring the clock pins. Subtasks 8 and 9 were verified by use of the Xray Debugger in a stand alone PC connected to the prototype board by a RS-232 cable (8 bits data, 1 stop bit, no parity, 9600 Baud) and monitoring program execution. Results were displayed on each device's display screen and no hardcopy test results were generated from these devices.

There were some difficult areas associated with the prototype testing. These include the TPU phase controls, the 5 msec timer, and the synchronous communications link. These turned out to be primarily software issues, not hardware. The 68332 microcontroller is configurable to such a degree that the main issues associated with causing the circuit to behave in a manner that is desired are related to the software programming.

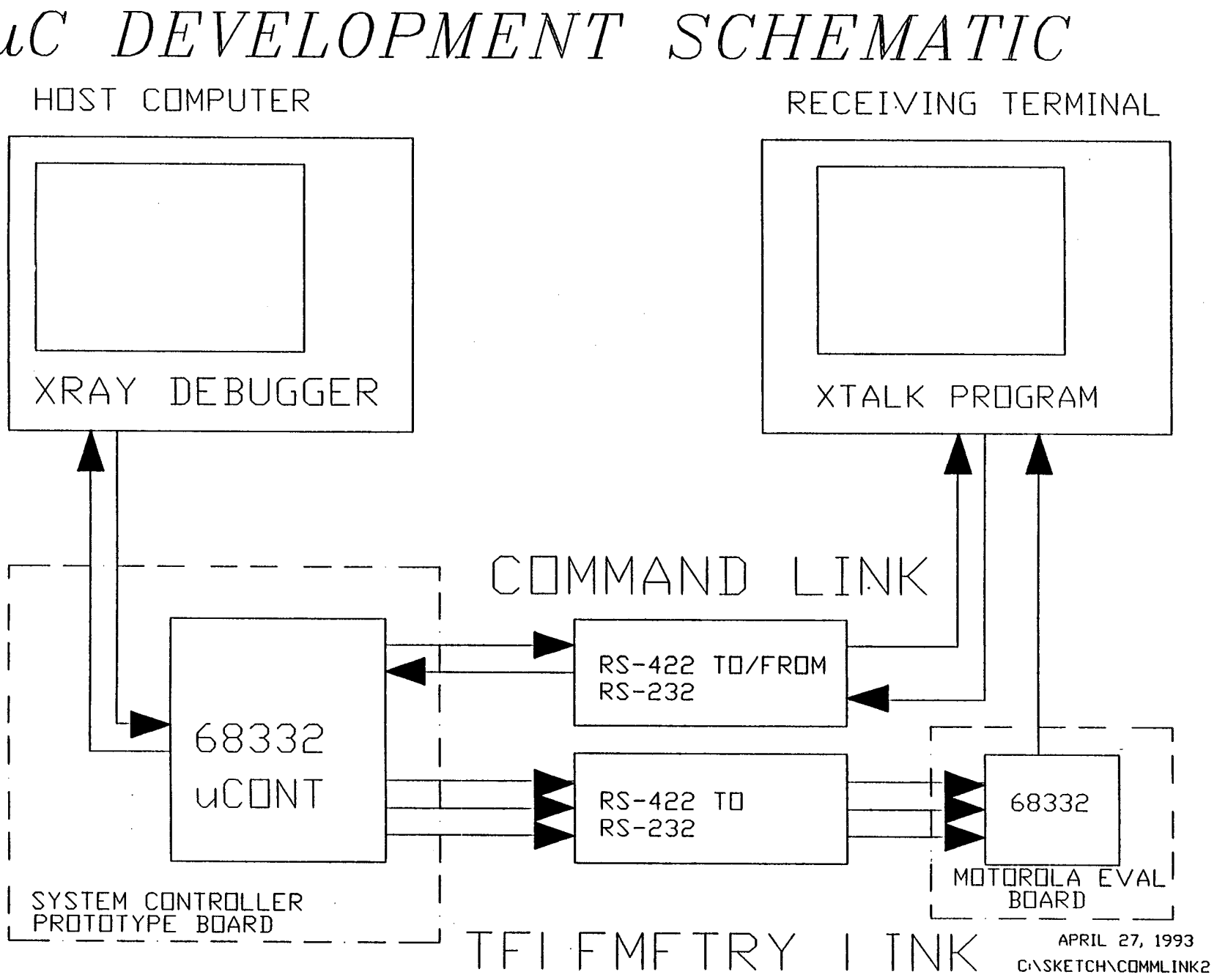
uC DEVELOPMENT SCHEMATIC
HOST COMPUTER
RECEIVING TERMINAL
XRAY DEBUGGER
XTALK PROGRAM
COMMAND LINK
68332
uCONT
RS-422 TO/FROM
RS-232
RS-422 TO
RS-232
68332
SYSTEM CONTROLLER
PROTOTYPE BOARD
MOTOROLA EVAL
BOARD
TFI FMFTRY I TNK
APRIL 27, 1993
C:\SKETCH\COMMLINK2

Figure 1

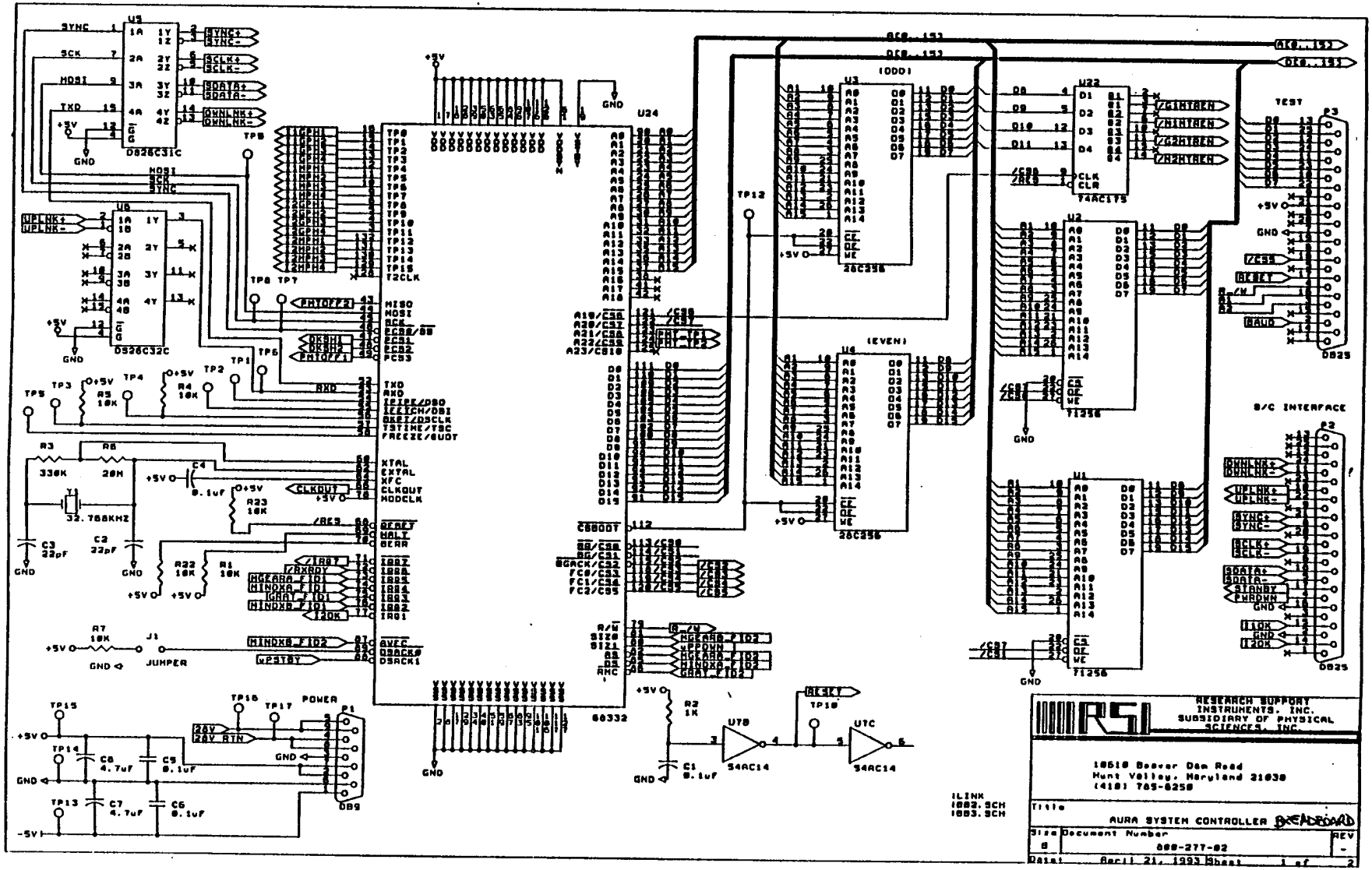
RESEARCH SUPPORT INSTRUMENTS, INC.
SUBSIDIARY OF PHYSICAL SCIENCES, INC.
10616 Beaver Dam Road
Hunt Valley, Maryland 21030
(410) 785-6259
Title
AURA SYSTEM CONTROLLER BREADBOARD
Size B
Document Number 888-277-02
REV -
Date: April 21, 1993 Sheet 1 of 2
ILINK 1882.SCH 1883.SCH
(ODD)
(EVEN)
TEST
S/C INTERFACE
POWER
JUMPER
DB25
DB9
26C256
T4AC175
T1256
54AC14
68332

Figure 2

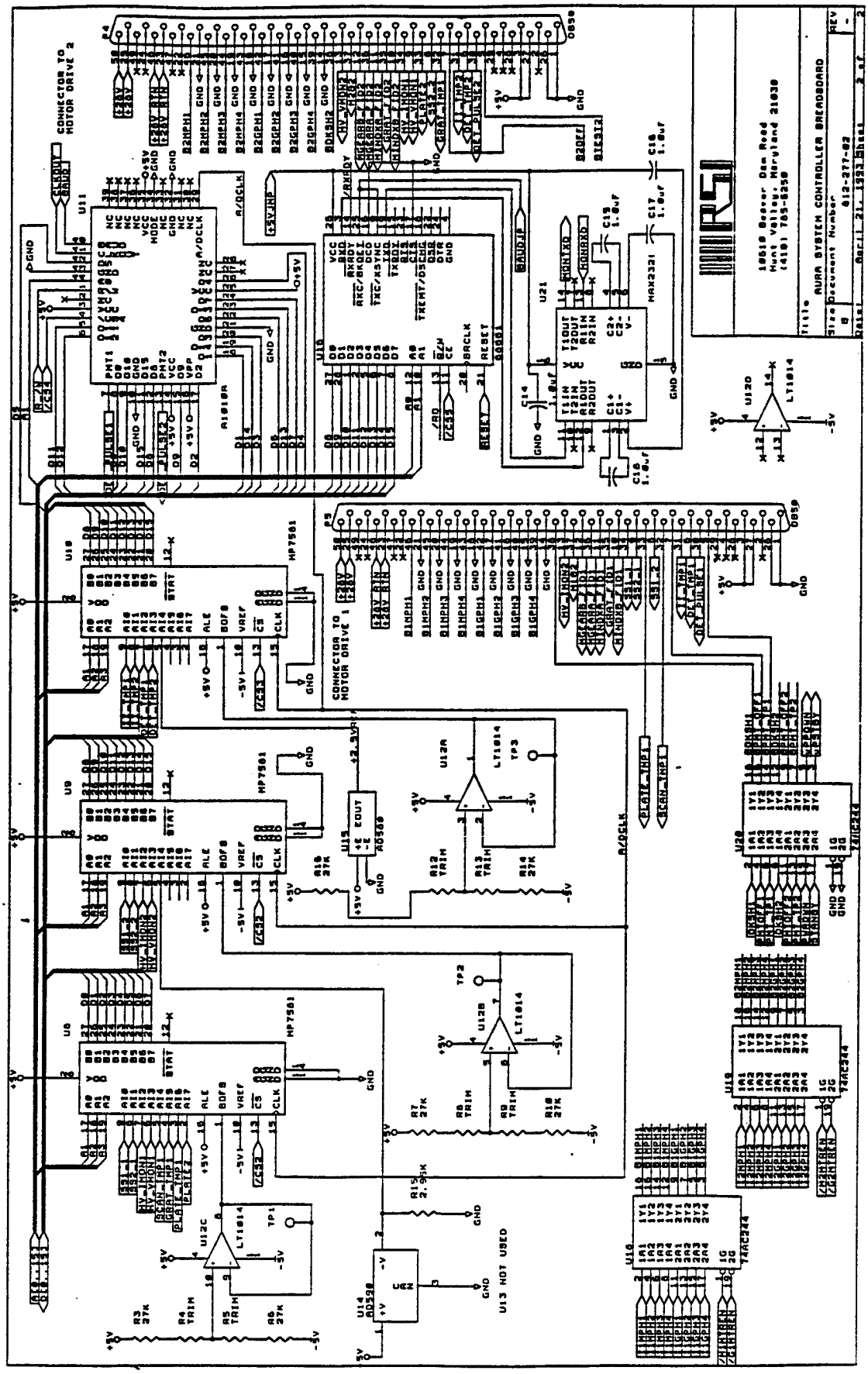

Figure 3

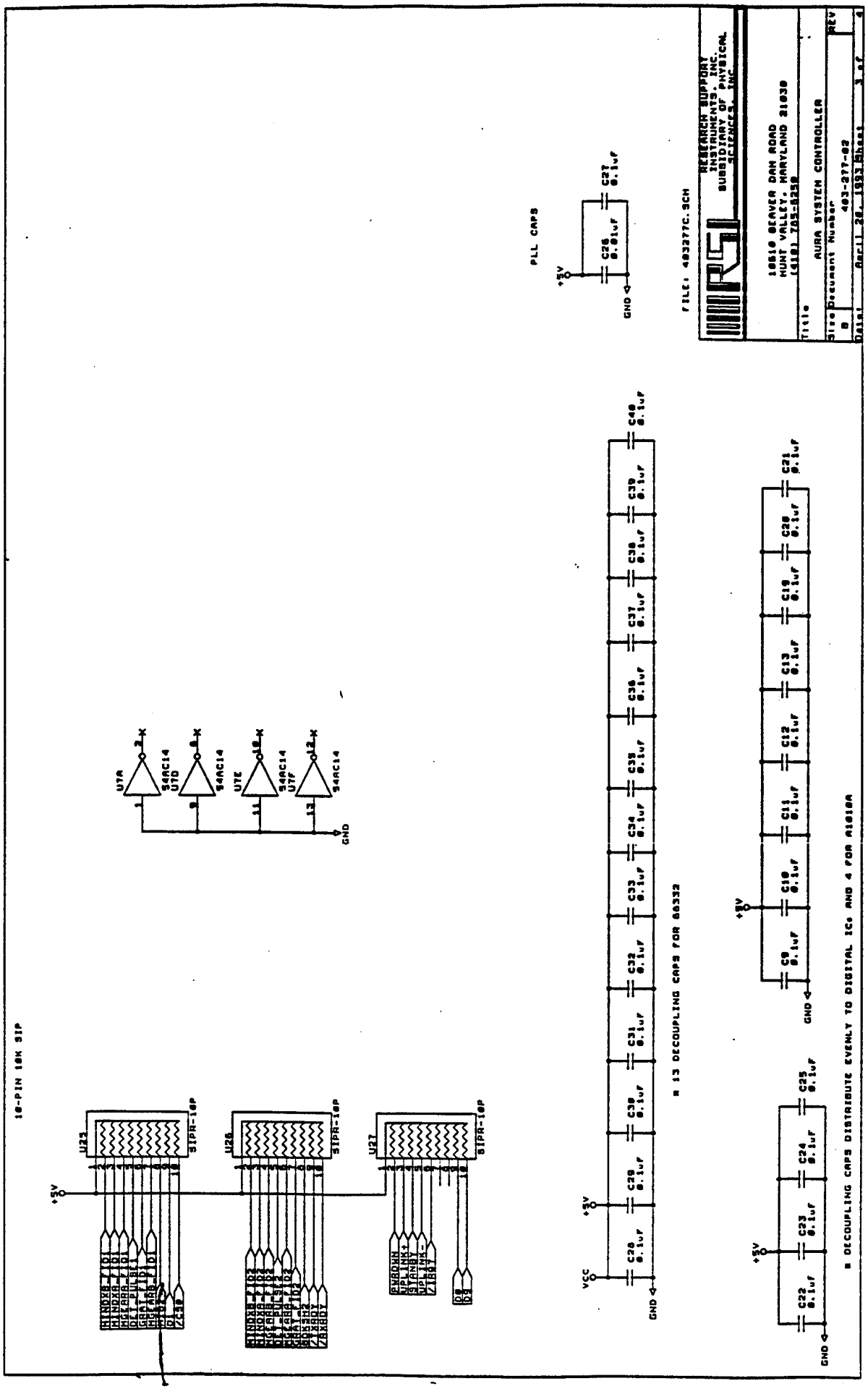
16-PIN 16K SIP
U23
U26
U27
SIPR-16P
+5V
GND
U7A
U7D
U7E
U7F
54AC14
PLL CAPS
C25 0.1uF
C26 0.01uF
C27 0.1uF
FILE: 403277C.SCH
RESEARCH SUPPORT INSTRUMENTS, INC.
SUBSIDIARY OF PHYSICAL SCIENCES, INC
10810 BEAVER DAM ROAD
HUNT VALLEY, MARYLAND 21030
(410) 785-8259
Title
AURA SYSTEM CONTROLLER
Size
Document Number
403-277-02
REV
Date: April 28, 1993 Sheet 3 of 4
= 13 DECOUPLING CAPS FOR 80332
= DECOUPLING CAPS DISTRIBUTE EVENLY TO DIGITAL ICs AND 4 FOR A16BA

Figure 4

(blank)

Appendix E

Thermal Analysis of the Pulse Amplifier/Discriminator Board in the Integrated Detector Assembly

1.0 Introduction

The pulse amplifier-discriminator (PAD) of our integrated photon detectors consists of six transistors and seven integrated circuits on a small printed circuit board. There has been some speculation that the devices on this PCB might reach intolerable temperatures when operated in vacuum, despite the modest power level (0.25 W maximum). I have analyzed the thermal characteristics and determined that the PCB will in fact rise to excessive temperatures when operated in vacuum. The temperature rise can be limited to tolerable values by either modifying the detector housing to promote radiative coupling to the walls, or by using a multilayer PCB with a copper ground plane to provide conductive coupling to the housing. The latter yields the most reliable thermal control for this PCB.

2.0 Method of Analysis

The computer program used to analyze the temperature rise distributions on printed circuit boards is based on achieving energy conservation at all points on the board. The PCB is divided into a number of square segments. A table is written compiling the heat production in each segment, the direct thermal conductances from that segment to the housing, and the thermal contacts to adjacent segments. If the thermal conductivity of the PCB, including coatings and metallization, is K, and the board thickness b, then the conductance linking adjacent segments is the product Kb, and the heat flow between two segments is $(T_1-T_2)Kb$. If the ith segment has power generation P_i and conductance to the environment H_i, the energy balance equation is $P_i-T_iH_i+Kb\Sigma(T_j-T_i)=0$, where the summation is taken over the adjacent segments j. Where an adjacent segment does not exist, i.e., along edges, the term is omitted.

Boundary conditions are handled through the environment conductances H_i. A point on the board that is thermally grounded, through a metal standoff or other thermal link, is assigned a large value of conductance.

The program makes an initial guess at the temperature distribution, then computes the power flows into and out of all the segments for that distribution. The temperature of the segment with the largest heat flow value is then adjusted to achieve zero heat flow, taking the adjacent segment temperatures to be unchanged. This is the temperature distribution for the next iteration. The innermost loop of the computer program repeats this process as many times as there are segments.

The mean temperature of the PCB is calculated and compared, in the next order loop, to that of the previous iteration. When that mean temperature changes by less than 0.02 degrees upon execution of the inner loop, the program ends.

3.0 Thermal Excursions of the Unmodified PCB

The PAD PCB is a double-sided board, 1 mm thick. Both sides are etched, and the residual copper is sparse. The absence of a ground plane layer causes the effective thermal conductivity of the board to be very low. Allowing for a double (board top and bottom) layer of Conathane, 0.020" thick, the overall board thickness is 2 mm and the effective (average) thermal conductivity, 0.00138 W/cm-K.

The PCB is L-shaped, with power regulation circuitry at the top of the L (Figure 1). A rectangular array of 0.74 cm squares is superimposed on this shape to define the segments for the thermal calculation.

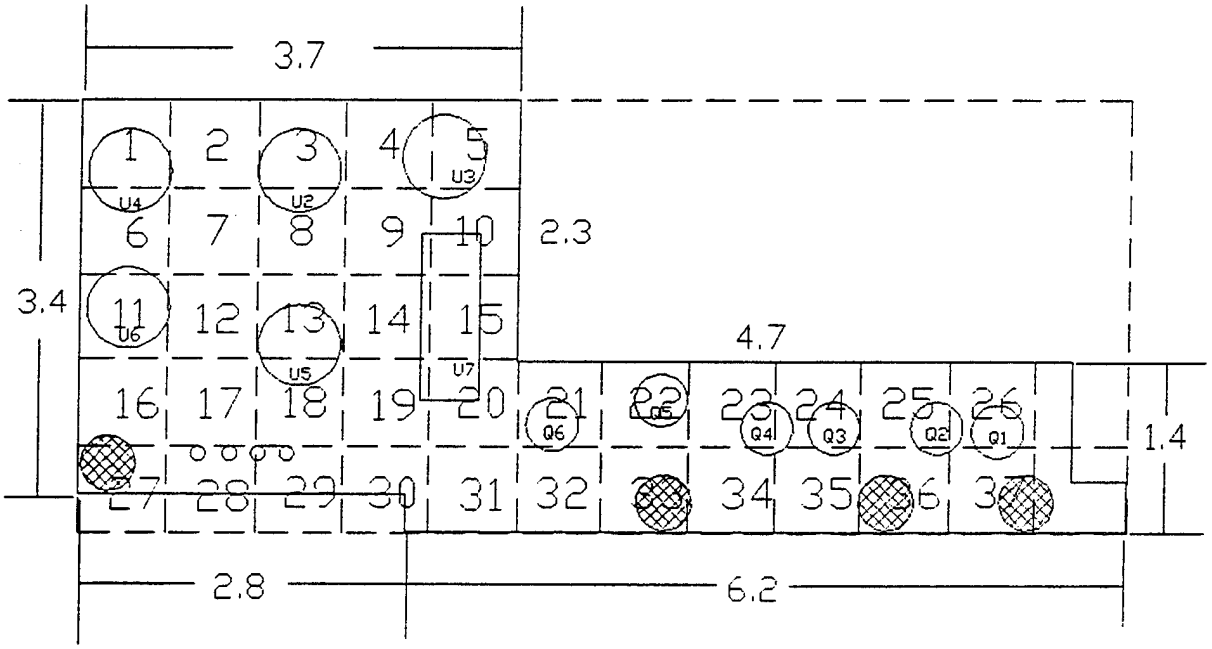

Figure 1. PCB dimensions (cm) and division into 0.74 cm squares. Hatched areas indicate swaged standoff points.

Various integrated circuit and transistor devices are shown. The ICs at segment 5 and segment 11 are thermally grounded with thick layers of conductive compound. These points, and the standoff points of segments 27, 33, 36, and 37, are assigned thermal conductances of 10 W/K. This value is arbitrarily chosen, and is simply large enough to yield zero temperature rise at these locations.

There are also 4 #24 wires connected from segments 28-29 to a connector, with lead lengths on the order of one inch. The thermal conductance of each of these links is about 0.003 W/K.

There are other connections to this board, but these have been neglected for the current calculation, on the assumption that they are too long to be significant. Refinements can be easily incorporated into the model if warranted.

The power consumption of the electronics is about 125 mW idling, rising to 250 mW at high count rates. No single component dominates the power consumption; the 54LS221, for example, draws 23 mW. I assumed a simplified model for the distribution of heat generation on the board, taking a uniform distribution over the PCB area of 19.7 cm^2 (excluding the power regulator segment, #5), or 12.7 mW/cm^2 at maximum power.

Neglecting thermal radiation, the equilibrium temperatures are as shown below, where the relationship between indicated temperatures and PCB location should be self-evident.

100.8	104.8	99.0	70.8	0.0						
71.8	89.6	96.4	88.3	68.3						
0.0	60.2	83.6	92.8	91.5						
22.6	42.7	60.0	82.6	88.4	75.1	52.3	56.6	52.2	35.9	30.5
0.0	3.0	6.2	64.3	79.2	59.8	0.0	40.3	39.2	0.0	0.0

Clearly temperature regulation by thermal conduction through the board to the standoffs alone is poor. There are, however, other contributions to heat removal to consider.

4.0 Radiative Heat Elimination

The PCB is mounted in a metal chamber, the top facing the top plate of the detector, the bottom of the board facing an interior wall. Since thermal conduction is very weak, it is plausible that radiation would be a significant means of thermal coupling to the housing. This would be most effective for a thermally black housing.

The housing is in fact made of nickel-plated aluminum, which will be highly reflective in the thermal infrared. The thermal emission from the PCB is largely reflected back onto the board, substantially reducing the effectiveness of radiative cooling. A fraction $(1-\epsilon_2)$ of the thermal emission from the PCB will be reflected back from the housing wall. A fraction ϵ_1 of this will be absorbed by the PCB, and the remainder re-reflected toward the housing walls. An infinite series of terms for the multiple wall reflections is easily written down and, being a simple power series, is explicitly summed. A bit of manipulation yields an expression for the effective PCB emissivity: $\epsilon = \epsilon_1\epsilon_2/(\epsilon_1+\epsilon_2-\epsilon_1\epsilon_2)$. The thermal emissivity of the aluminum walls of the housing will be very low, probably less than 0.05. Then the effective PCB emissivity, assumed to be on the order of 0.85, is reduced to 0.0496, or essentially ϵ_2.

The fourth-power law of thermal radiation can be linearized for small deviations around a reference temperature T_0, in this case the housing temperature. This yields a thermal conductance coefficient H given by $4\sigma\epsilon AT_0^3$, where σ is the Stefan-Boltzmann constant (5.67×10^{-12} W/cm^2-K^4), A is the segment area, and ϵ is the net PCB-housing thermal emissivity. This is doubled to account for two PCB faces. This thermal coupling coefficient for the PAD PCB then evaluates to 2.7×10^{-5} W/K. Then the equilibrium temperature rise distribution is:

54.9	57.1	54.5	40.0	0.0						
40.2	50.0	53.8	49.8	39.3						
0.0	35.4	47.9	52.7	52.1						
15.9	27.0	35.9	48.0	51.3	45.1	33.3	37.6	35.7	25.7	22.5
0.0	2.2	4.1	38.3	46.6	36.1	0.0	27.7	27.3	0.0	0.0

Compare the values without thermal radiation; evidently radiation is quite significant in reducing the temperature rise of the PCB.

These temperatures are not inconsistent with observation. The only test data deal with a measurement at segment 17, for which the calculation shows a 27 degree temperature rise. The tests are done with zero signal, which reduces PCB power by half, so a 13-14 degree temperature rise is expected. The measured temperature rise at this point, in vacuum, is said to be 10-12 degrees (specific data are absent; one must depend on the experimenter's memory).

The calculation has neglected the residual copper metallization of the PCB. This will reduce the maximum temperatures above.

5.0 Assessment of the Current PCB Design

The model indicates that, under the worst case condition of a high photon signal rate, temperatures as high as 50-55 degrees above case temperature may be generated. If the housing is at an elevated temperature, the local PCB temperature may exceed 90°C. Junction temperatures will be slightly higher.

The devices used are rated to operate at temperatures well above 90°C, so nothing should fail as a consequence of these high temperatures. However, device lifetime and reliability are degraded rapidly with increasing temperature. Reducing the PCB temperature, while not essential for instrument performance, is advisable for maximum reliability and lifetime.

6.0 Thermally Black Housing

One measure that could be taken without changing the PCB is blackening the interior of the housing. This might be done by using anodized aluminum instead of nickel plated, or by coating the walls with a good infrared black, such as Aquadag.

If the PCB surface (Conathane) has $\epsilon_1=0.85$, and the walls have $\epsilon_2=1$, with $T_0=300$ K, and $A=0.55$ cm^2, the thermal conductance from each segment to the black walls is 5.7×10^{-4} W/K. The temperature rise of the PCB for radiative coupling to high-emissivity walls is:

11.3	11.6	11.4	9.4	0.0						
9.4	11.0	11.5	11.0	9.4						
0.0	9.2	11.0	11.5	11.3						
6.6	8.5	9.5	11.1	11.4	10.9	9.2	10.6	10.5	8.7	8.3
0.0	1.3	1.6	9.6	10.9	9.3	0.0	8.8	8.8	0.0	0.0

This is, or would be, clearly highly effective at limiting the PCB temperature rise to tolerable values. Even with the housing hot, at 40°C, the maximum PCB temperature will be an acceptable 51°C.

7.0 Ground Plane Enhanced Thermal Conductance

As noted above, providing a thermally black housing in place of the nickel-plated housing would reduce these temperatures substantially. There are some difficulties with obtaining such a thermally absorbing coating. Anodizing, for example, entails additional work in taping to preserve conductive areas for preserving shielding and grounding. A black coating might be applied, but could be a source of outgassing.

One easy and very effective way to increase thermal conductance between the PCB and the housing is to use a multilayer PCB with a ground plane. The copper layer greatly enhances the thermal conductance between the isolated portions of the PCB and the metal standoffs. If a single ground plane of one-ounce (1 oz/ft^2) copper is incorporated, the average thermal conductivity of the PCB is increased from 0.00138 W/cm-K to 0.066 W/cm-K, almost a fifty-fold increase. This is an indication of how poor the thermal conductivity of PCB materials is.

The thermal conductance of the copper is so high that radiation becomes insignificant. The temperature distribution of the PCB, with radiation to the nickel-plated, low-emissivity housing, is as follows:

2.1	2.2	2.1	1.5	0.0						
1.5	1.9	2.1	1.9	1.5						
0.0	1.4	2.0	2.2	2.1						
0.6	1.4	1.9	2.2	2.1	1.7	1.1	1.1	1.0	0.7	0.6
0.0	1.0	1.6	2.1	2.0	1.4	0.0	0.8	0.8	0.0	0.0

Now the temperature rise is quite insignificant, only a few degrees above the housing temperature. This is a 25-fold improvement over the current arrangement, and a factor 5 better than the temperature rise obtained with radiative coupling to a thermally black wall.

8.0 Conclusion

The PAD PCB provides poor heat sinking by thermal conduction, due to the absence of a ground plane layer. Thermal radiation would be adequate for this low power circuit if the PCB were in an enclosure with high thermal emissivity walls. The actual wall materials have very low emissivity, which practically eliminates thermal radiation cooling. In vacuum, at high signal rates, device temperatures may be on the order of 50 degrees above ambient. While not exceeding any component ratings, such temperature rises significantly degrade component reliability and lifetime.

Either the PCB should be modified with a ground plane for thermal conduction to the standoffs, or the metal walls should be treated for high thermal emissivity, to achieve adequate cooling. The ground plane might well improve the stability of the pulse amplifier-discriminator. The PAD can now be stabilized only by grounding the circuit to the chassis, an arrangement which causes difficulties in spacecraft since this violates proper grounding procedure.

The current system is not well designed for use in vacuum, developing temperatures which, while not immediately fatal, will degrade the lifetime and reliability of the detector electronics.

9.0 Addendum

The calculations above neglected the trace metallization of the PCB. An inspection of the layout indicated that the total area of traces (counting only linear segments, not isolated pads) is about 5% of the PCB surface area of each side, or 10% total. The copper deposition is nominally 2 ounces per square foot, or 680 μm thickness. Modeling the traces as a random distribution (the computer model cannot handle anisotropic thermal conductances), this is taken to be equivalent to 68 μm of copper uniformly distributed on the PCB. The effective thermal conductivity of the PCB with this layer of copper is 0.0145 W/cm-K, or more than ten times the conductivity without the copper.

This clearly makes a very great difference to the temperature distribution:

10.0	10.4	9.9	7.1	0.0						
7.1	9.0	9.8	9.0	7.0						
0.0	6.4	9.0	9.8	9.5						
2.6	5.3	7.5	9.3	9.4	7.8	5.2	5.5	5.0	3.4	2.9
0.0	2.3	4.0	8.1	8.7	6.3	0.0	3.9	3.8	0.0	0.0

Evidently there is no thermal problem with this board, with or without a ground plane.